Exploring the conformational binding mechanism of fibrinogen induced by interactions with penicillin β-lactam antibiotic drugs.

Michael González-Durruthy[1,2*], Ramón Rial[1], M. Natália D. S. Cordeiro[2], Zhen Liu[3], Juan M. Ruso[1*]

[1]Soft Matter and Molecular Biophysics Group, Department of Applied Physics,University of Santiago de Compostela, 15782 Santiago de Compostela,Spain.
[2]LAQV@REQUIMTE/Department of Chemistry and Biochemistry, Faculty of Sciences, University of Porto, 4169-007 Porto, Portugal.
[3]Department of Physics and Engineering, Frostburg State University, Frostburg, Maryland 21532, United States.

*Corresponding author: juanm.ruso@usc.es, gonzalezdurruthy.furg@gmail.com

Keywords: Fibrinogen, β-lactam antibiotics, molecular docking, ANM models, spectroscopic methods.

Abstract

Herein, we present an integrated computational and experimental study to tackle the interactions between recognized β-lactam antibiotics (cloxacillin and dicloxacillin) with the fibrinogen blood plasma protein. For this purpose, molecular docking simulation with elastic network based on collective low-frequency normal modes and perturbation response scanning maps were proposed to evaluate the conformational binding mechanism of fibrinogen under the unbound and bound states with the cited β-lactam antibiotics. Aiming to theoretically explore the hidden biochemical mechanisms and structural attributes leading failures in therapy success with β-lactam antibiotics. The computational results pointing that despite these conformational differences, both antibiotics exhibit very similar affinity-based free energies of binding as FEB (cloxacillin/E-region) = - 8.7 kcal/mol and FEB (dicloxacillin/E-region) = -7.7 kcal/mol. We theoretically suggest that the semi-synthetic incorporation of an additional halogen CL-atom in the dicloxacillin, respect to cloxacillin molecule, and its relative docking-pose orientation in the fibrinogen E-region could significantly reduce the appearance of potential fibrinolytic off-target effects usually associated to parenterally administered β-lactam antibiotics. Besides, the performed interactions diagrams revealed that the most relevant antibiotic binding interactions with the fibrinogen E-region (pocket 1) are mainly

based on hydrophobic (C···C)-backbone-side-chain non-covalent interactions, acceptor/donor interactions with critical regulatory E-region residues SER50:Q > SER50:N associated to allosteric modulation based long-distance-based perturbations (dicloxacillin >> cloxacillin) in the E-region (Q-chain > N-chain) with remarkable conformational rigidification by decreasing the intrinsic collectivity, and leading different pattern of perturbations as allosteric signal propagation in the intrinsic conformational dynamics under bound state from both β-lactam antibiotics. An experimental validation was carried out by using calorimetric (ITC and DSC) and spectroscopic (Raman and fluorescence) methods. These methods corroborated the computational results, adding quantitative information to explain the binding process. Finally, the obtained results open new perspectives for the "*de novo rational drug-design"* of new derivatives of β-lactam antibiotics with high pharmacodynamic selectivity/specificity to avoid side-effects toward to achieve optimal benefit/risk rates beyond the antibiotic drug resistance phenomena, favoring the implementation of rigorous criteria for a more personalized antibiotic therapy.

Introduction

Despite the enormous attention that for so many years have enjoyed by the scientific community protein-ligand interactions, far from diminishing, has increased the interest and fascination that this topic exercise upon researchers. Many are the causes that explain such an attraction: multidisciplinary approach, constant discovery of new proteins and ligands, the recent emergence of COVID-19 with the consequent demand for new vaccines and medicines[1], the development of artificial intelligence methods that are nurtured by large databases[2], the excellent combination of thriving tools both experimental and computing that this field more than others need to coexist [3] and the scientific challenge that the complexity of these systems (dynamic, fluctuations, degrees of freedom, crowding, etc.) assumes[4].

Penicillin β-lactam antibiotics are recognized as one of the most common wide-spectrum antibiotics used for different infections. However, the therapy success with penicillin β-lactam antibiotics remains as unsolved problem since β-lactamase resistance due to the inappropriate use, is disseminating rapidly among pathogenic bacteria. Besides, considering the occurrence of potential hematotoxicity (off-target fibrinolytic

interactions) as hemolytic anemia caused by intravascular hemolysis, and blood clotting disorders-mediated fibrinolysis (i.e., by interactions with the fibrinogen molecule) which are recognized as one of the most severe adverse reactions induced by the penicillin β-lactam antibiotics when are parenterally administered [5]. To overcome the potential hematotoxicity of the β-lactam antibiotics therapeutic strategies should consider the rational prescription, substitution and/or combination [6].

In pursuing these aims, we have studied the interactions and complexation of two penicillin β-lactam antibiotics, cloxacillin and dicloxacillin, with the fibrinogen serum protein. We have attempted to correlate the effects of chemical substitution on molecular and thermodynamic properties of protein in the bulk with their effects on protein functional properties. The penicillin drugs selected for study form an interesting series of molecules in which the only variation in the molecular structure is the number and nature of the substituents on the aromatic ring: an additional chlorine atom on the phenyl ring of dicloxacillin. This selection provides an interesting opportunity to investigate the relationships of the molecular structure on the intermolecular interactions[7-9]. In previous studies we investigated the relationships between molecular architecture and the physicochemical properties of structures that are formed by these molecules in aqueous solution. Static light scattering and NMR studies have shown that both drugs form small aggregates from a given concentration in aqueous solution, but there was evidence of a second aggregation in solutions of dicloxacillin (but not cloxacillin)[10]. The stability of these aggregates has not yet been quantified sufficiently, but it has highlighted its enormous importance on the bacterial activity [11] and protein interactions, where evidence has been presented for the haptenation of penicillin by conjugation with serum proteins which results in the formation of IgE antibodies [12, 13]. From the structural and functional point of view the human fibrinogen is a soluble glycoprotein composed by disulfide-linked dimer of three nonidentical polypeptide chains, Aα, Bβ, and γ. The NH_2 terminal portions of the six chains are linked together to the central region (E) of the molecule by 11 disulfide bonds forming a small globular domain, the so-called disulfide knot, in the center. The C termini of each of the three chains end in globular domains, those of the Bβ, and γ chains are located at the ends of the molecule. The COOH- terminal portion of each fibrinogen Aα chain forms a compact αC-domain attached to the bulk of the molecule with a flexible αC-connector. In addition, fibrinogen shows a unique characteristic in its folding[14]. According to the current view, in fibrinogen, two αC-domains interact intramolecularly with each other and with the central region of the

molecule, while in fibrin, they switch to an intermolecular interaction to form αC-polymers. The central region (E-region) is responsible for the fibrin polymerization during the clotting process[15]. Fibrinogen circulates in the plasma with a molecular weight of ~340 kDa depending of Aα and Bβ chains and the γ-γ and α-α crosslinking chains content. It has a shape similar to a rod with dimensions of 9 × 47.5 × 6 nm and present a negative net charge with isoelectric pH=5.8 in physiological conditions[16]. The normal concentration of fibrinogen is around 150–400 mg/dL in the blood plasma. Levels noticeably below or above this range are associated with pathological conditions like bleeding and/or thrombosis [17]. Crystallographic analysis of the molecule has been hindered for a long time by its complex and flexible structure. Finally, a planar sigmoidal structure was proposed: the axis of the α-helical coiled-coil rod adopts a sigmoidal shape that lies nearly in a plane, as the curvature is an intrinsic feature of fibrinogen's coiled coil [18].

In order to achieve these objectives and based on all the above, we have approached this task with a combination of experimental and computational methods. Spectroscopic (circular dichroism, UV-VIS, fluorescence, dynamic light scattering) and calorimetric (differential scanning and isothermal titration) techniques have been selected for their capabilities to determine the energies that take place in the interaction processes and the structural, morphological and conformal changes that the molecules undergo. With regard to computational methods, molecular docking approaches has become an increasingly important and recognized tool in rational drug-design[19] The molecular docking simulation can be applied to model the interaction between a small molecule and a protein receptor at the atomic level, allowing to efficiently elucidate keys biochemical processes [20]. Despite the existence of great advances in computational pharmacology are still ignored how different binding-modes can modulate the pharmacological response. The molecular docking results generally suggest that the native binding-mode corresponds to a low free energy structure but not necessarily with the lowest values. In this regard, one of the main challenges, is to implement computational algorithms that allow to discriminate correctly the influence of a given conformational binding-modes of the ligand on the interaction energy (FEB values), which are usually, very close to each other[21]. Because, in most cases the different ligand-conformations obtained after the molecular docking simulations occupy the same biophysical environment in the protein binding-site. For this instance, the local perturbation response scanning maps (LPRS map images) could be considered as an

efficient approach to identify differences-based penicillin-conformational binding-modes with fibrinogen protein[22, 23]. The LPRS maps allows the determination of the influence/sensitivity that each binding residue has on/to every other residue under ligand interaction, by performing a map-based matrix of interaction that works with an anisotropic network model (ANM), where the nodes refer to individual residues[24, 25].

Materials and Methods

Materials

Bovine plasma fibrinogen, fraction I, type IV, was purchased from Sigma and used as received. Sodium cloxacillin [5-methyl-3-(*o*-chlorophenyl)-4-isoxazolyl penicillin] and sodium dicloxacillin [3-(2,6-dichlorophenyl)- 5-methyl-4-isoxazolyl penicillin], and nafcillin sodium [6-(2-ethoxy-1-naphthamido) penicillin] were obtained from Sigma Chemical Co. The buffer solution used was 50mN glycine plus sodium hydroxide to give a pH of 8.5. Samples were prepared within 2 h prior to using. All chemical reagents were of analytical grade and solutions were made using doubly distilled and deionized water.

Differential scanning calorimetry

Differential scanning calorimetry (DSC) measurements were performed using a VP-DSC (MicroCal Inc., Northampton, MA) calorimeter with 0.542 ml twin cells for the reference and sample solutions. Prior to the DSC experiments, the samples and the references were degassed under vacuum while being stirred. Thermograms were recorded between 20 and 110 ºC at a scan rate of 60 ºC per hour. To check the reproducibility, each experiment was repeated three times. The baseline reference, obtained with both cells filled with buffer, was subtracted from the thermograms of the samples. The heat capacity curves were evaluated using the MicroCal Origin 7.0 software to obtain ΔH and T_m values.

Isothermal titration calorimetry.

Experiments were carried out in a VP-ITC microcalorimeter (MicroCal Inc., Northampton, U.S. [26]. To determine the binding isotherms, the drug solutions were introduced into the syringe (296 μL), while the fibrinogen solution 0.033 mM were introduced into the sample cell (1.416 mL). The stirring was kept constant at 416 rpm.

An important factor to consider is the equilibrium time necessary before starting each experiment, in our case it was one hour, more than enough for the power base line to remain stable. Injections of 10 μL at a constant rate of 0.5 μL s^{-1} were performed every 300 s. To eliminate negative signals, a reference power of 25 μJ s^{-1} was applied. Thus, it is guaranteed that the signal is not altered by any overcompensation mechanism. Dilution experiments of pure drugs were also conducted. The values obtained were systematically subtracted from those measured for the fibrinogen-drug systems. In this way, it is guaranteed that all the heat produced in the cell is due solely to the binding process. Following the described procedure, experiments were performed at a temperature of 298 K.

Raman spectroscopy

The Raman scattering measurements were taken using a Raman microprobe instrument consisting of a Jobin–Yvon T64000 spectrometer equipped with a microscope, which allows a spatial resolution on the sample of about 1 μm. The Raman signal was detected by a multichannel CCD detector cooled with liquid nitrogen. Raman spectra over the whole optical frequency range were recorded using the subtractive configuration of the spectrometer, with a spectral resolution of about 2 cm^{-1}. To improve the resolution of closely spaced peaks, high-resolution scans of some frequency regions were recorded using the triple additive configuration, with a spectral resolution better than 1 cm^{-1}. The light was collected in backscattering geometry through an objective of numerical aperture 0.95. The 785 nm line of an Ar^{+} laser was used as excitation, focused on a spot of ≈1 μm in diameter, with an incident power on the sample of ≈2 mW.

Fluorescence measurements.

A Cary Eclipse spectrofluorometer was used to perform the fluorescence measurements. The emission and excitation splits were 5 nm. The data interval was set to 1 nm and the averaging time at 0,5 seconds. The synchronous fluorescence spectra of fibrinogen due to the presence of the aromatic residues were obtained within a range of 290-450 nm upon excitation at 280 nm. The temperature was fixed at 298.15 K maintaining the Fibrinogen concentration constant at 1 μM and increasing concentrations of BTS from 0 μM to 200 μM. (1, 2, 4,8, 10, 50, 100, 200 μM). UV-Vis-IR Spectral Software from FluorTools was used for data processing[27, 28].

Computational modeling-based molecular docking simulation.

To study the binding properties between the penicillin β-lactam antibiotics and fibrinogen protein a computational mechanistic study based on molecular docking simulation was performed. Towards such end, first we prepared the protein receptor file (*i.e.,* fibrinogen), which was withdrawn from the *RCSB Protein Data Bank* (PDB) X-ray structures, *i.e.* with *PDB ID*: 1JY2 [29]. Afterwards, the obtained fibrinogen E-region structure was prepared using an online *ProteinPrepare* tool [30]. The preparation process includes the titration of the protonation states using *PROPKA 3.1 tool*, addition of missing atoms, removal of co-crystallized ligands and overall optimization of the H-network using *PDB2PQR 2.1*. Following this step, the penicillin β-lactam antibiotic ligands (cloxacillin and dicloxacillin) were obtained from the *Pubchem Data Base Chemical Structure Search* as cloxacillin (PubChem CID: 6098; MF: 435.9 g/mol) and dicloxacillin (PubChem CID: 18381; MF: 470.3 g/mol) [16]. The drugs geometry optimization was carried out by using the MOPAC extension based on NDDO approximation [31]. Then, to study the β-lactam antibiotic docking mechanisms with fibrinogen, we used the Autodock Vina scoring function developed by Trott *et al*.[32, 33] to obtain the free energy of binging (FEB) based on X-Score function which approximates the standard chemical potentials. Before the docking modeling, the fibrinogen binding-sites were predicted through the ezPocket with *fconv* for binding-site detection [34, 35]. This step was carried out as delimiting the access to fibrinogen-cavities, like van der Waals surfaces that are likely to bind to the ligands. To this end, the *fconv* analysis uses Delaunay triangulation with weighted points to detect all the relevant binding pockets. Herein, the volumetric map of the fibrinogen binding-site is generated together with the Cartesian *XYZ*-coordinates for the docking box simulations [36], *i.e.*: grid box size with dimensions of X= 64Å, Y= 52Å, Z= 52Å and grid box center X= 13.1Å, Y= -2.0Å, Z= 12.5Å. For this purpose, a docking accuracy was fixed at 100 and after that, the best conformations or penicillin binding-poses were selected [33]. The docking affinity (FEB values) were classified like energetically-unfavorable when the FEB of fibrinogen-penicillin complexes ≥ 0 kcal/mol, therefore indicating either extremely low or complete absence of affinity; otherwise the fibrinogen-penicillin docking complexes were classified like medium to high docking affinity [32].

Performing 2D/3D Lig-Plot interaction diagrams.

This algorithm was applied to evaluate the influence in the FEB values for the different contributions of the β-lactam antibiotics binding-poses interacting with the

fibrinogen. To specify the key relevant intermolecular interactions 3D Lig-Plot diagrams were analyzed. To tackle this objective, the ezLigPlot software was used. This software determines the non-covalent intermolecular interactions present in a given protein-ligand complex and it builds automatically a 3D-interaction diagram that includes hydrophobic, H-bond, cation-Π, and Π-Π stacking interactions along with its corresponding interatomic distances (d_{ij}) for each binding-poses from the obtained docking complexes [37].

Building perturbation response scanning maps based on elastic network models.

This computational approach evaluates the degree of change (*i.e*., interatomic distances perturbation between residue fluctuations) induced by the ligands in the residues network of fibrinogen by describing the interaction potential (V) from the receptor-ligand complex (R-L or fibrinogen-β-lactam antibiotics) as an anisotropic network model (ANM) of interacting springs based on the Elastic Network Model Theory (ENM) [23, 38-40], where each spring connects a pair of C(α)-nodes (i-j) corresponding to the ligands (*i.e.,* (i)-cloxacillin or (i)-dicloxacillin) and the receptor (j-fibrinogen) are placed within a given distance cutoff of 7 Å. Herein, we use the ANM models applying the concepts on rotation-translations blocks approximation (RTB model) to explore the collective motions in low-frequency normal modes. Where the target protein (fibrinogen) is splitted into n-(b)-blocks, a block being made of one or of a few consecutive residues that belong to the different polypeptide chains of the fibrinogen protein that could potentially interact with the penicillin β-lactam antibiotic ligands (cloxacillin and dicloxacillin). Then, the ANM-RTB model was implemented to evaluate the potential perturbation responses-induced by the β-lactam antibiotics on fibrinogen binding-site network of residues using local perturbation-response scanning maps (LPRS maps) to measure the fluctuations of the displacements from equilibrium between the unperturbed (unbound fibrinogen) and perturbed state (bound fibrinogen under the β-lactam antibiotic interactions) following **equations 1** and **2**:

$$V_R = \sum_{(i<j)\in N(R)} \frac{1}{2}\gamma_R \left(d_{ij} - d_{ij}^0\right)^2 \quad (\mathbf{1})$$

$$V_{R-L}^{'} = \sum_{(i<j)\in N(R)\cup N(L)} \frac{1}{2}\gamma_R \left(d_{ij} - d_{ij}^0\right)^2 + \sum_{(i,j)\in N(R,L)} \frac{1}{2}\gamma_L \left(d_{ij} - d_{ij}^0\right)^2 \quad (\mathbf{2})$$

Where V describes the interaction potential for a protein receptor (*i.e.,* V_R: fibrinogen in the unperturbed like unbound state representing the intrinsic conformational dynamic in

the absence of the penicillin β-lactam antibiotic ligands), and the bound state representing the interaction-based perturbations (*i.e.,* $V_{R\text{-}L}$: fibrinogen/cloxacillin and fibrinogen/dicloxacillin as generated docking complexes) modeled by a quasi-harmonic Hookean springs [41]. For this instance, the force constant (γ) of the spring connecting C(α)-atoms *i* and *j* from the receptor (interacting residues) and the ligand are taken as γ_R and γ_L respectively. See **equation 3**:

$$\gamma = exp\left[\left(-1/2\right)\left(\left(d_{ij}^{0}/d_{cutoff}\right)^{2}\right)\right] \quad (3)$$

The cutoff for the fibrinogen $\gamma_R = 1$, d_{ij}^0 is the distance between i,j-C(α)-atoms of the β-lactam antibiotic as ligand (*L*) and fibrinogen receptor (*R*), in the equilibrium condition indicated by the superscript "0", and the d_{cutoff} = 7 Å. More details will be explained in the next section.

Results and discussion

Computational section

Fibrinogen structural characterization and binding site prediction

The accurate identification of druggable binding pockets constitutes an essential step for structure-based drug design antibiotics considering the long list of biochemical mechanisms associated to antibiotic-resistance phenomena[42]. Which is widely recognized as a fundamental public health threat affecting humans worldwide. In this context, the first step of molecular docking approach is the correct prediction/identification of a feasible binding pockets with an appropriate crystallographic structural characterization of their properties toward to ensure quality of modeling data as ligand selectivity and specificity in order to avoid adverse effects[34]. In the present study we address the prediction of druggable fibrinogen binding sites considering the fibrinogen whole structure (E-region, D-region 1 and D-region 2) in order to determine the highest concentration and patterns of distribution of active binding sites throughout the fibrinogen structure. Following this idea, the binding-sites prediction of fibrinogen was carried out by applying fpocket with ezPocket software which use Voronoi tessellation algorithm to detect/scanning concave surfaces and tiny sub-cavities

(tunnels) collecting information-based on the crystallographic descriptors related to pocket topology and geometry to accommodate the ligands (cloxacillin and dicloxacillin) with favorable interactions. See **Figure 1.**

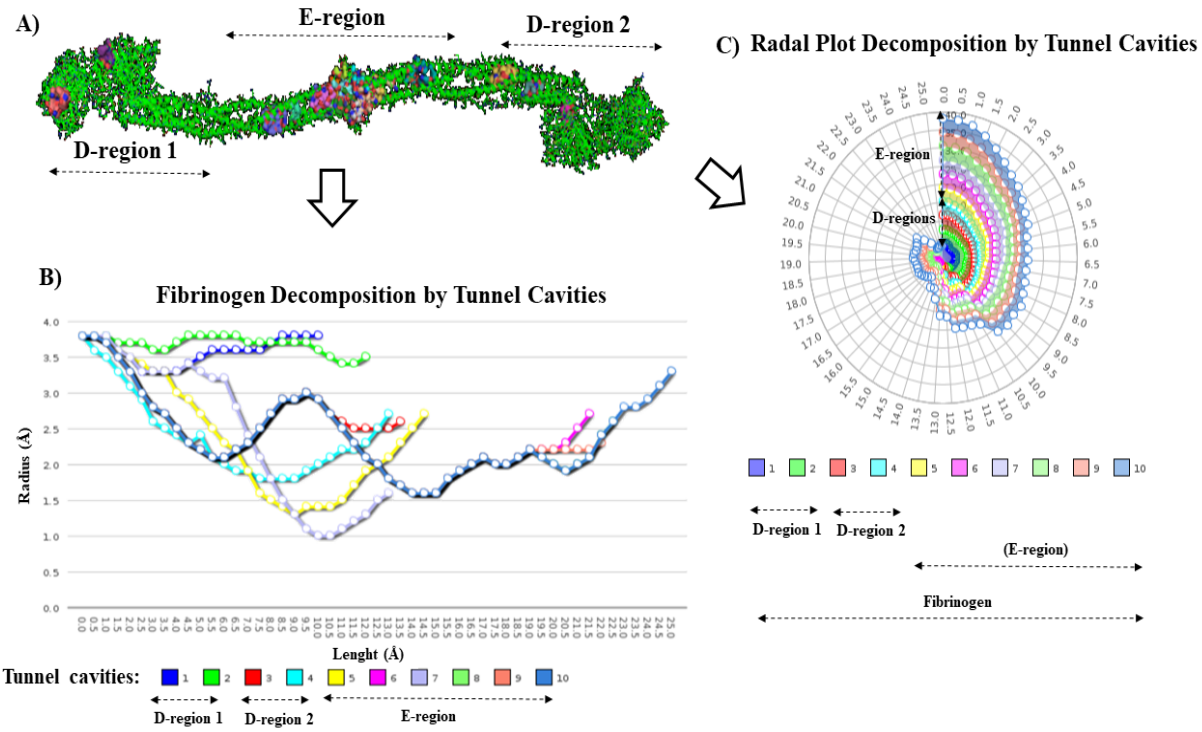

Figure 1. A) Representation of general crystallographic structure of fibrinogen protein by relevant regions formed by two quasi-symmetric C-terminal portions (D-regions 1 and 2) and the central part (E-region thrombin binding-domain) highlighting the binding sites formed by small cluster of hydrophobic cavities represented as colored van der Waals surfaces heterogeneously distributed across the overall structure. B) Graphical representation of length (Å) vs. radius (Å) obtained for the fibrinogen tunnel sub-cavities (10 entangled tunnels) belonging binding sites for each fibrinogen regions (E-region and the two quasi-symmetric D-regions 1 and 2). C) Radial plot decomposition of the tunnel sub-cavities of the fibrinogen binding sites showing the overlaping within the each fibrinogen region.

For this instance, the fpocket method calculates the geometric center of the pocket and considering if the relative position of the pocket center is within 4 Å from any atom of the potential ligand to be considered as correctly predicted or identified. The fpocket

binding cavity detection method can generates cartesian coordinates-like van der Waals volumetric maps that allows setting the box-simulation used for docking experiments [36]. The obtained results show that the fibrinogen protein has multiple cavities more densely located in the N-terminal central nodule E-region which correspond to the thrombin binding-domain which has critical importance for the blood coagulation process (fibrin polymerization). By the other hand, the regions composed by the two quasi-symmetric C-terminal portions showed the smallest quantity of binding sites (D-region 2 > D-region 1). In addition, we perform a detection of tiny sub-cavities (or tunnels) composing fibrinogen binding sites for each region [17, 43]. For this instance, a total of 10 relevant tunnels were identify, 6 interconnected tunnels composing the E-region binding sites, and 2 tunnels for each D-region binding sites. Herein, was clearly shown that the number of tunnel cavities forming the E-region binding sites are greater than the tunnel cavities composing from both D-regions. Furthermore, the length and radius of the tunnels composing the E-region binding sites are also significantly higher than the D-region sub-cavity tunnels as showed in the **Figure 1B** and **Figure 1C**. This fact has great relevance from the pharmacological point of view on prevention potential hematotoxicity effects-mediated fibrinolysis which are considered as one of the most severe adverse reactions induced by penicillin β-lactam antibiotics, immune-mediated hemolytic anemia [5], and intravascular hemolysis induced by off-target ligand interactions with tunnel sub-cavities of fibrinogen binding sites. Because, it is well-known that the critical functions of the tunnels include: i) substrate and solute exchange, ions and water between the sub-cavities, ii) transport of intermediates of biochemical reactions between two different binding sites, and iii) maintenance of the conformational and geometric complementarity of binding sites for binding physiological substrates [44]. Afterward, in order to assess the biochemical relevance of the three main regions of the fibrinogen structure (E-region, D-region 1 and D-region 2) we examine three relevant pocket descriptors which are directly associated to the protein ability to bind potential drugs namely: i) pocket stability (Ps_fib), ii) pocket continuity (Pc_fib), and iii) pocket correlation ($Pc_{i\text{-}j}$_fib)[45]. The stability parameter of the fibrinogen binding pockets belonging to the cited regions can be calculated according to the following **equations 4** and **5**:

$$P_{s\_fib} = \{S_1, S_2, \dots, S_i, \dots, S_m\} \quad (4)$$

$$S_i = {}^{n}/_{N} \quad (5)$$

where P_{s_fib} represents the fibrinogen pocket stability; S_i corresponds to the stability of the grid formed by the pocket; the parameter m represents the number of grids in the fibrinogen pocket, n is the number of occurrences of the i-th grid in the pocket conformations, and N is the total number of the pocket conformations. The results on the stability parameter of the fibrinogen molecule are depicted in the **Figure 2.**

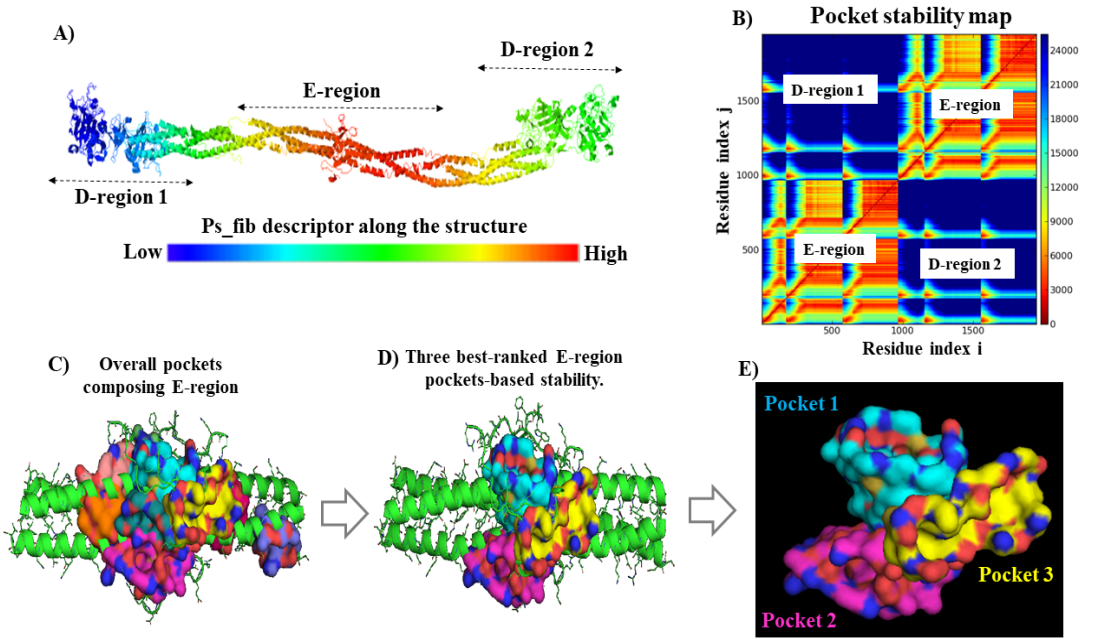

Figure 2. A) Representation of the stability properties of fibrinogen binding pockets based on the Ps_fib crystallographic molecular descriptor; from low to high stability as depicted by the bar color (from blue to orange). **B)** 2D-matrix of pocket stability map based on the Ps_fib parameter by relevant fibrinogen regions. **C)** Representation of overall pockets (10 pockets in total) composing the E-region like van der Waals surface. **D)** and **E**) van der Waals representation of the three best-ranked fibrinogen E-region pockets with the highest stability (pocket 1 > pocket 2 > pocket 3 > remaining E-region pockets >>> D-region 2 > D-region 1).

For the fibrinogen E-region, 10 pockets in total were detected across the E-region surface while for the D-region 1 and 2, 2 and 4 pockets were detected, respectively. See (**Figure 2A**). According to this the fibrinogen E-region suggest could has greater influence for ligand-binding affinity compared with the two D-regions. Particularly, in

the E-region the central pocket 1 forms a funnel-shaped hydrophobic cavity that exhibits the greatest stability of all the E-region binding sites detected. Theoretically suggesting that the pocket 1 represents the intrinsic binding pocket for the dynamic and functional properties of the fibrinogen protein. This pocket 1 is surrounded by the pockets 2, 3 and 4 and the stability analysis showed that the pocket 2 and 3 are slightly more stable than the pocket 4. **Figure 2C** (labelled-orange van der Waals surface). Maybe the pockets 2 and 3 provide an allosteric pathway for the antibiotic-ligand entry and exit to the main pocket 1. Besides, considering that pockets 2 and 3 cover a large surface of the central segment of E-region. The pockets (5, 7, 8) could also be considered like potential allosteric binding pockets allowing accommodate small ligand molecules. Due to their relative position respect to the funnel-shaped hydrophobic cavity that forms the main pocket 1. The remaining pockets (pockets 6,9, and 10) could act binding small molecules as several co-factors and other native substrates during the binding of thrombin into the E-region for the fibrin polymerization during the blood coagulation process based on based on its lower stability compared with the pockets 1, 2 and 3. Herein, it is important to note that the stability of the predicted pockets composing the D-regions were from medium to very low pocket stability. See **Figure 2A**.

The fibrinogen binding pocket continuity (P_{c_fib}) [45], was analyzed based on general structural attributes as appearance, merging, and volume change. The continuity descriptor is defined by the **equation 6**:

$$P_{c\_fib} = \{P_i | P_i \cap P_{ref} > 0\}, i = 1, 2, \dots, n \quad (6)$$

where, P_{ref} represents the evaluated pocket in the first or native conformation, P_i corresponds to the *i*-th pocket which is spatially overlapped with the P_{ref} , n represents all the predicted pockets modeled, and P_{c_fib} denotes the binding pocket continuity consecutively assembled pockets. This parameter (P_{c_fib}) is strongly depends on the proximity of the pockets, and on their flexibility properties which are associated to the different conformations that these pockets can adopt under the presence or absence of ligands (penicillin β-lactam antibiotics). Besides, the pocket continuity descriptor can be associated with the pocket correlation parameter ($P_{ci\text{-}j\_fib}$) through a correlation matrix[45]. For this instance, we reinforce our hypothesis about the greatest relevance of

the fibrinogen E-region compared with the two D-regions 1 and 2. Due to the high structural inter-connection between the pockets that form the E-region (i.e., for the 10 binding pockets) compared with the less quantity and low structural communication observed for both D-regions. Besides, considering the strong correlation based on the high values for the parameter **(**$P_{ci\text{-}j\_fib}$**)** for the E-region compared with both D-regions 1 and 2. Where the pocket correlation parameter **(**$P_{ci\text{-}j\_fib}$**)** for both fibrinogen D-region**s** shows several parts with moderate correlation as average values of $P_{ci\text{-}j\_fib}$ (colored-white) to full uncorrelated low $P_{ci\text{-}j\_fib}$ values (colored-blue), see **Figure 3.**

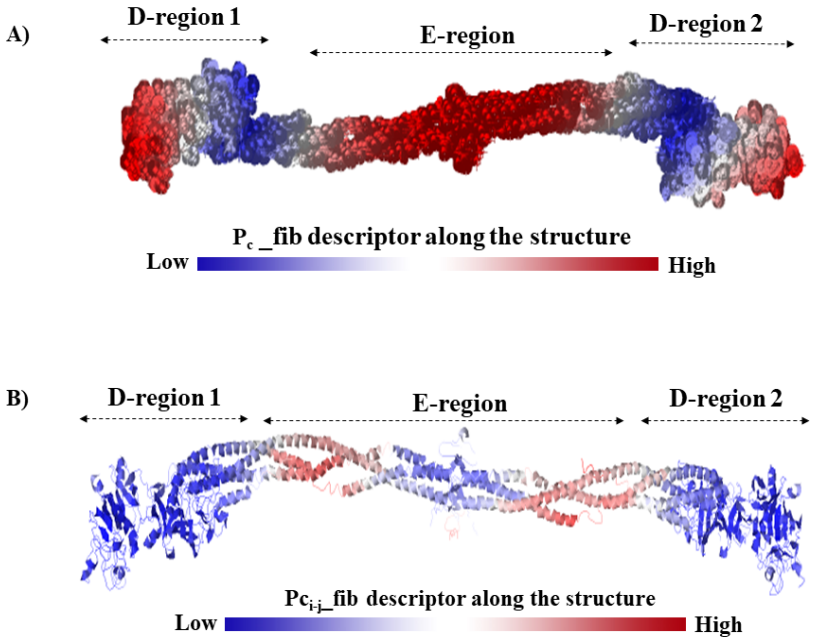

Figure 3. A) Representation of the pocket continuity crystallographic molecular descriptor (P_{c_fib}) by fibrinogen regions (E-region, D-region 1 and D-region 2). **B)** Representation of the pocket correlation crystallographic molecular descriptor ($P_{ci\text{-}j\_fib}$) for the evaluated fibrinogen regions. The bar color is to qualitatively represent the values of the crystallographic molecular descriptor evaluated as low, average, and high values according to the color intensity (blue-to-white-red transitions).

Molecular Docking Simulations

Considering all the above we performed the molecular docking simulations focus our attention on the potential docking interaction between the penicillin β-lactam antibiotics (cloxacillin and dicloxacillin) with the fibrinogen E-region, see **Figure 4**.

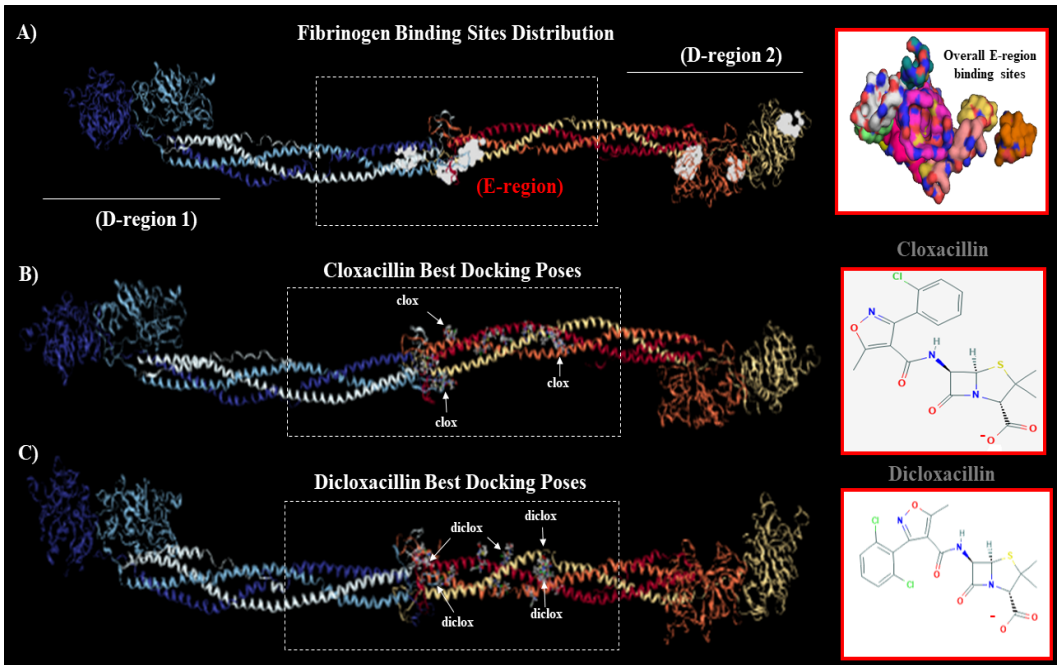

Figure 4. **A)** Fibrinogen binding sites distribution from more to less densely located by relevant regions as white volumetric surfaces (E-region > D-region 2 > D-region 1). On the far right is represented overall the binding sites that form the fibrinogen E-region. **B)** Representation of the best crystallographic docking poses obtained for the fibrinogen-cloxacillin complexes, and **C)** representation of the best crystallographic docking poses obtained for the fibrinogen-dicloxacillin complexes showing greater affinity for the region E. On the far right is represented the chemical structure of both β-lactam antibiotics cloxacillin and dicloxacillin, respectively.

From the structural point of view, the fibrinogen E-region binding-sites are highly complex systems which contain a large variety of clefts, grooves, protrusions inner the main funnel-hydrophobic cavity (pocket 1) formed by the γ-γ and α-α crosslinking from Aα and Bβ chains composing the thrombin binding site [43]. Under the presence of ligands (cloxacillin and dicloxacillin), some critical residues can be perturbed by modifications in the symmetry architecture of the Bβ-γ/Bβ-γ dimeric domain of E-region and could induce potential hematotoxicity effects-mediated like fibrinolysis when these antibiotics are parenterally administered [5]. In general terms, the obtained results suggest that the antibiotic interactions fit with a spontaneous thermodynamic process (ΔG bind < 0 kcal/mol). Pointing the formation of stable docking complexes with the several predicted fibrinogen E-region binding sites. As showed in the **Figure 4B** and **Figure 4C**

where the best crystallographic docking poses were centrally located around the funnel-shaped hydrophobic cavity, namely the main pocket 1 previously identified like the most stable pocket. Then, aiming to deepen the modeling results, we carried out a clustered docking analysis involving the three fibrinogen regions studied, see **Figure 5**.

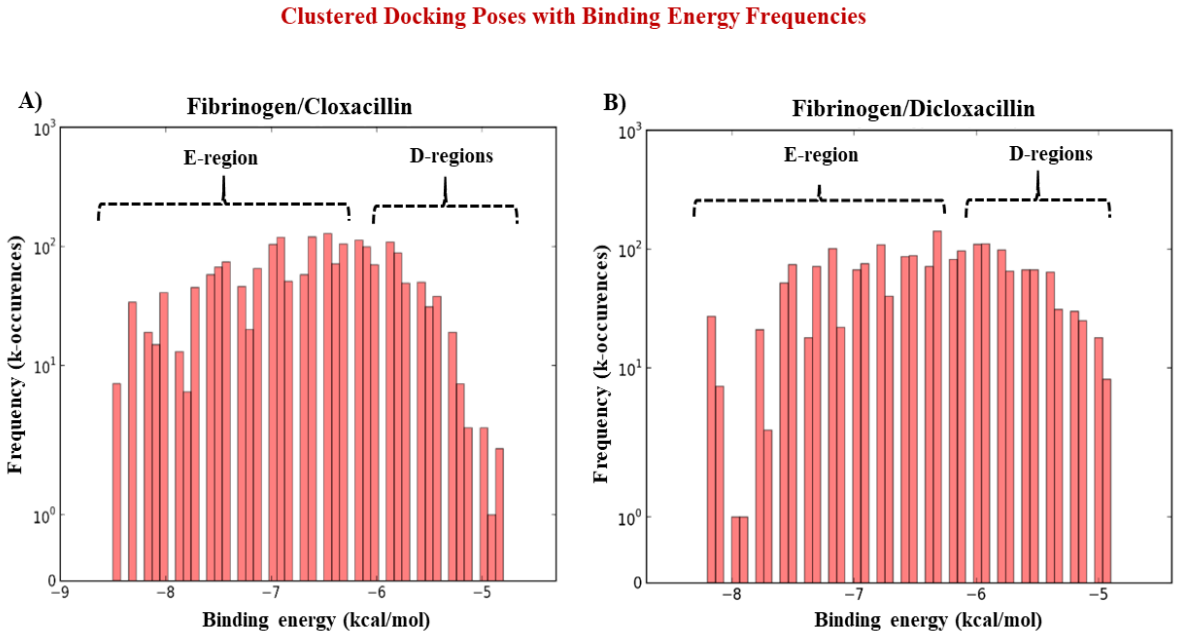

Figure 5. Frequency distribution of total binding energies from the docking complexes obtained for both β-lactam antibiotics by relevant regions (E-region and D-regions) as: **A)** fibrinogen-cloxacillin complex and **B)** fibrinogen-dicloxacillin complex. Herein, the x-axis represents the total affinities (ΔG_{bind_total}) and y-axis ordinate represents the frequencies (k-*occurrences) of* ΔG_{bind_total} values (kcal/mol) obtained for all docked poses by fibrinogen regions (*pink bars).*

The results showed in the **Figure 5** corroborates that the antibiotic binding interactions occur with a higher binding probability in the fibrinogen E-region compared with the two D-regions regarding the count of binding affinity frequencies (k-occurrences)[46]. In fact, the calculated values of the k-occurrences in fibrinogen E-region (k = 10-100) were higher compared with the values of k-occurrences of interactions for both penicillin β-lactam antibiotics in the D-regions (k = 20-50), approximately, which denote the preference of the cloxacillin and dicloxacillin by the central fibrinogen E-region, in both cases.

In order to theoretically explain the pharmacodynamic mechanisms of interactions for cloxacillin and dicloxacillin with the fibrinogen E-region and detect potential similarities and differences from the structure-fibrinogen activity relationships point of view a detailed 3D/2D-lig-plot interaction diagrams were performed for both antibiotics [37]. See **Figure 6**.

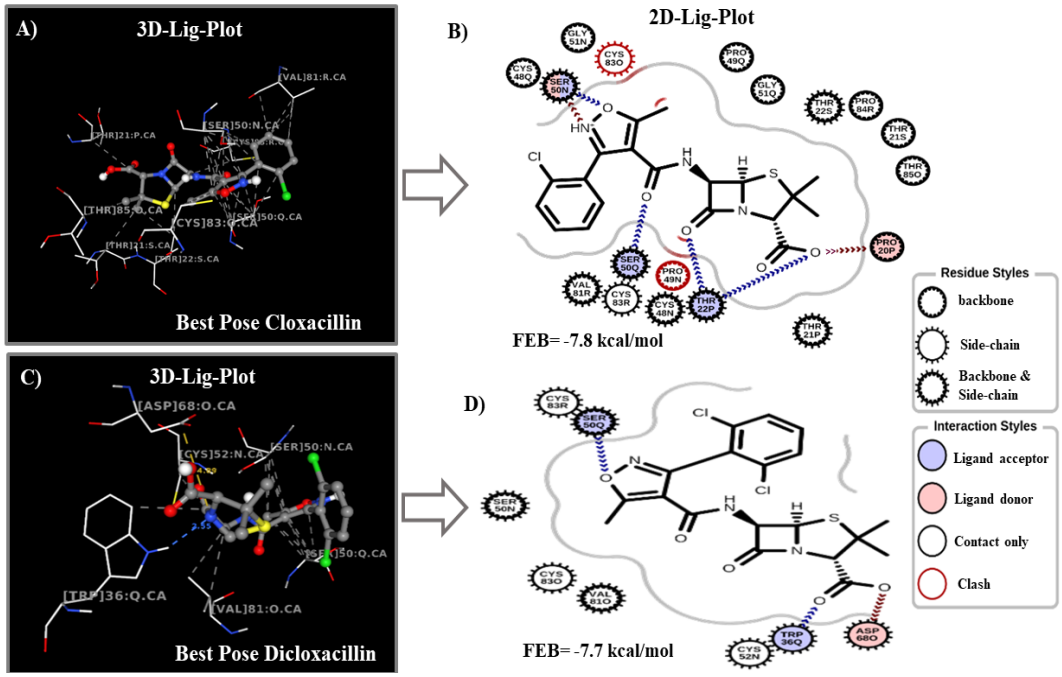

Figure 6. Representation of 3D and 2D lig-plots interaction diagrams for the best β-lactam antibiotic binding-poses obtained in the fibrinogen E-region like: **A-B**) fibrinogen-cloxacillin and **C-D**) fibrinogen-dicloxacillin. On the far right is depicted the different types of hydrophobic interactions of the ligands with the fibrinogen E-region target residues and chains as: ligand/side-chain interactions, ligand/backbone-side chain interactions, and electrostatic interactions as: ligand/backbone acceptor, ligand/backbone donor, ligand/side-chain acceptor, ligand/side-chain donor; the gray outline represents the proximity contour of the 2D lig-plots interaction diagrams. Please, note the different crystallographic orientation of the CL-atom(s) of the cloxicillin and dicloxicillin during the interactions marked in green in the obtained 3D-lig-plot diagrams. More details can be found in **Figure SM1** and **Figure SM2**.

Herein, it is possible to note that, the cloxacillin molecule involves a greater number of E-region target-residues covering a greater area in the E-region biophysical

environment (pocket 1) compared with the dicloxacillin molecule; despite the similar structural size of both antibiotics. This fact could be explained due to in the case of cloxacillin, the best binding pose (cloxacillin/E-region) shows an extended shape. However, the dicloxacillin ligand adopts a more closed conformation during the docking interaction. An overview of the results of 3D/2D-lig-plot diagrams revealed that the most relevant antibiotic binding interactions with the fibrinogen E-region (pocket 1) are mainly based on hydrophobic (C···C)-backbone-side-chain non-covalent interactions, involving a greater number of these for the cloxacillin >> dicloxacillin. In this regard, we suggest that the presence of less quantity of hydrophobic (C···C)-backbone-side-chain non-covalent interactions for the dicloxacillin could promotes a decrease of the thermodynamic destabilizing effects on the residue side-chain packing of the E-region (pocket 1) [47, 48], potentially inducing a minor quantity of local perturbations over the interacting chains composing the E-region and without affect the flexibility properties and ligand-binding properties of the fibrinogen. Consequently, this dicloxacillin chemical modification (Cl-atom addition) contributes to prevent potential immune-mediated hemolytic anemia, intravascular hemolysis, and the most representative the effects namely fibrinolysis more efficiently way than the cloxacillin molecule. As showed in the 2D-lig-plot diagrams (panel B and D) the β-lactam ring is the most important toxicophoric fragment inducing side effects (off-target interactions) of β-lactam antibiotics (cloxacillin >> dicloxacillin) on fibrinogen. Toxicophoric groups, correspond to chemical motifs within a molecule responsible for the appearance of fibrinolytic side-effects leading defects in the blood clotting process[5].

From the therapeutic point of view, it is important highlight that the β-lactam ring is the pharmacophoric fragment responsible for the specific antibiotic action for both evaluated drugs (*i.e.,* in the absence of off-target interactions with fibrinogen blood plasma protein)[5]. In this context, the 2D-lig-plot diagrams show that the β-lactam ring belonging to the cloxacillin exhibits a large number of hydrophobic (C···C)-backbone-side-chain non-covalent contacts with fibrinogen E-region residues and chains (PRO49:Q, GLY51:Q, THR22:P:S, PRO84:R, THR21:P:S, THR85:O:R) compared with the dicloxacillin where the β-lactam ring has a unique hydrophobic (C···C)-backbone-side-chain non-covalent contact with the fibrinogen E-region residues and chains (CYS52:N). According to this, we could hypothesize several events associated with the β-lactam ring linked to the loss of selectivity/specificity, and greater potential of the cloxacillin molecule respect to dicloxacillin to induce potential hematotoxicity

(fibrinolytic side-effects) like: i) total or partial perturbation of the cys-stereochemical orientation of the H-atom pair of the β-lactam ring, ii) total or partial loss of the strain in the bicyclic system that form the four membered β-lactam ring. Particularly, the β-lactam carbonyl group must be placed in the correct orientation to provide the strain required for the attack-based acylation reaction of the β-lactam carbonyl group with the target-enzyme family (transpeptidases) and to remain the β-lactam ring stability against the action of β-lactamases. Besides, an efficient rational drug-design of penicillin β-lactam antibiotics with optimal benefit/risk ratio requires of the amidic character of the β-lactam carbonyl group to be reduced, to enable the acylation of the active nucleophilic serine residue (SER) of the transpeptidases. Then, slight distortions in the β-lactam carbonyl group orientation induced by the interaction with the fibrinogen protein (i.e., regulatory serine residue from fibrinogen E-region) could decrease the β-lactam ring strain opening the β-lactam ring and abolish its pharmacological properties (antibiotic effects). In this concern, it is well-known that the higher strain in the β-lactam ring increase the antibiotic activity and decrease the fibrinolytic hematotoxicity [5].

A similar analysis based on the orientation of chemical pharmacophoric groups can be performed for the CH3-groups composing the thiazolidine-5-membered nitrogen saturated ring which could be partially perturbed in their pharmacological trans-cys-stereochemical orientation after hydrophobic (C···C)-backbone-side-chain non-covalent contacts with E-region residues and chains (PRO84:R, THR21:S, THR85:O), this perturbation conformational event not occur for the dicloxacillin molecule. Besides, 2D-lig-plot diagrams show a greater presence of backbone-side-chain acceptor interactions > backbone-side-chain donor interactions happening in the oxygen atoms that form part of the β-lactam ring of both antibiotics (cloxacillin > dicloxacillin). In the case of cloxacillin the backbone-side-chain donor interaction occurs between the ionized oxygen atom with the PRO20:P and with the ASP68:O for the dicloxacillin. This oxygen atom forms part of the carboxylic group of cloxacillin and is important to selectively bind to positively charged nitrogens of the lysine from bacteria transpeptidase enzyme. By the other hand, we show that the carbonyl group composing the thiazolidine-5-membered nitrogen saturated-ring and the amide-oxygen that form part of the neighboring acylamino side-chain of the cloxacillin strongly interact with the regulatory fibrinogen E-region residues (SER50:Q and TRH22:P) through backbone-side-chain acceptor interactions. However, in the case of dicloxacillin molecule the a single backbone-side-chain acceptor interaction occurs between the carbonyl group composing the thiazolidine-5-membered nitrogen

saturated-ring with a non-regulatory fibrinogen E-region residue (TRP36:Q) which significantly decreases the occurrence of adverse effects (hematotoxicity-based fibrinolysis and coagulation defects) for the dicloxacillin. It is important to note that electrophilic carbonyl groups in both ligands favor nucleophilic attack to NH groups of regulatory fibrinogen residues like SER >> THR which present a crucial role in the phosphorylation processes during the thrombin bind to E-region which has critical importance for the blood coagulation process (fibrin polymerization).See **Figure SM3**
In addition, an interesting backbone-side-chain acceptor/donor triangular-shaped interaction between the O-atom and N-atom from the 5-membered isoxazolyl ring side-chain of the cloxacillin with high affinity for the regulatory fibrinogen E-region residue (SER50: N) was observed. This backbone-side-chain acceptor/donor triangular-shaped interaction was not observed for the dicloxacillin which showed weaker interaction involving only the regulatory E-region residue (SER50: Q). In this regard, it is important to highlight that the 5-membered isoxazolyl ring side-chain acts as steric shield but also favor the electron-withdrawing giving the structure acid stability modulating the β-lactam penicillinase resistance phenomena and hematotoxicity. According to this, the semi-synthetic incorporation of an additional halogen CL-atom in the dicloxacillin molecule, respect to cloxacillin significantly reduces the occurrence of primary and secondary fibrinolysis events respect to cloxacillin molecule through the action of strong negative inductive effects on the 5-membered isoxazolyl ring. This inductive-effect induce a notable weakening of the bonds between a hetero-atom (O, N) and a H-atom. Then, the electron-withdrawing group increases the acidity of the O-H bond of an acid (weakening of the O-H bond), but decreases the basicity of a nitrogen atom in an amine by decreasing the electron density in the free doublet allowing a more efficient modulation of the interaction properties when these β-lactam antibiotics are parenterally administrated. Besides, the differences observed in the relative docking pose-orientation in the E-region binding site for the CL-atoms of the dicloxacillin respect to single CL-atom from cloxacillin apparently is very important to maintain its pharmacological efficacy without compromising binding affinity of the formed docking complexes with very close FEB values as FEB (cloxacillin/E-region) = - 8.7 kcal/mol and FEB (dicloxacillin/E-region) = -7.7 kcal/mol.

Following the modeling procedures, we determine the total binding affinity (ΔG_{bind_total}) for each ligand, as well as their thermodynamic contributions (ΔG_{Gauss1}, ΔG_{Gauss2} , $\Delta G_{repulsion}$, $\Delta G_{H\text{-}bond}$, $\Delta G_{hydrophobic}$ and $\Delta G_{rotational}$ [46]). See **Figure 7**.

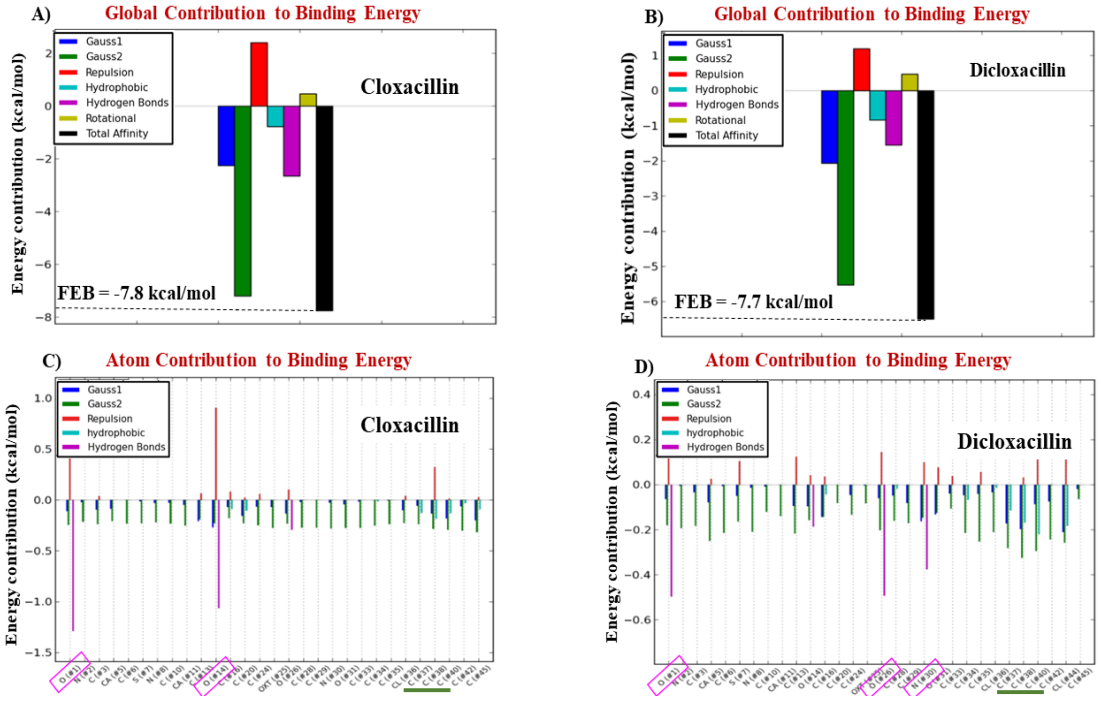

Figure 7. On the top, graphical breakdown of the global energy contribution to the total binding affinity (ΔG_{bind_total}) values (kcal/mol) obtained from the interaction of each β-lactam antibiotics with fibrinogen E-region like: **A)** fibrinogen-cloxacillin (ΔG_{bind_total} = - 7.80 kcal/mol) and **B)** fibrinogen-dicloxacillin (ΔG_{bind_total} = - 7.70 kcal/mol). Herein, different color-labels of the bars were used to indicate the type of thermodynamic contribution like: attractive energy dispersion based on two gaussian functions (Gauss1 and Gauss2 like blue and green, respectively), repulsion interaction energy (red), hydrophobic interaction energy (light blue), hydrogen bond energy (purple), rotational energy (yellow) and total binding affinity (black). On the bottom, graphical representation based on per atom energy contributions for each β-lactam antibiotic tested as: **C)** fibrinogen-cloxacillin and **D)** fibrinogen-dicloxacillin. Please, note that the symbol (#) *x-axis* was used only for labeling purposes not fitting with the atom-position in the β-lactam antibiotic ligand structures.

An overview of the molecular docking results showed in **Figure 7**, reveals that the most prevalent energy contributions to the total binding affinity (ΔG_{bind_total} = ΔG_{bind_Clox} + ΔG_{bind_Diclox}) from both β-lactam antibiotic drugs (ΔG_{bind_Clox} and ΔG_{bind_Diclox}) were associated to the contributions of the pair of steric Gaussian molecular mechanism distance-dependent terms (Gauss 2 and Gauss 1), which can be defined as

attractive terms of London dispersion forces[46]. In this sense, the Gauss 2 energy contribution provides relevant information on the influence of attractive binding energies of the docking complexes formed by the best docking pose of cloxacillin and dicloxacillin drugs with the fibrinogen E-region binding site (pocket 1). Herein, the procedure for obtaining the total binding affinity is according to the following **equations 7** and **8**:

$$\Delta G_{bind\_Clox} = (\Delta G_{Gauss1_{Clox}} + \Delta G_{Gauss2\_Clox)} + \Delta G_{repulsion_{Clox}} + \Delta G_{H-bond_{Clox}} + \\ + \Delta G_{hydrophobic\_Clox} + \Delta G_{rot\_Clox} \quad (7)$$

$$\Delta G_{bind\_Diclox} = (\Delta G_{Gauss1_{Diclox}} + \Delta G_{Gauss2\_Diclox)} + \Delta G_{repulsion_{Diclox}} + \Delta G_{H-bond_{Diclox}} + \\ + \Delta G_{hydrophobic\_Diclox} + \Delta G_{rot\_Diclox} \quad (8)$$

The results obtained for the Gauss 2 forces show the influence of strongest interactions with the fibrinogen E-region (pocket 1) based on non-covalent hydrophobic and non-electrostatic attractive energy contributions for both ligands evaluated and fitting well with the previous results. Herein, we strongly suggest that the high influence exerted by the Gauss 2 energy force ((Gauss 2_Clox > Gauss 2_Diclox), is due to temporary dipoles formation (fluctuating dipole–induced dipole) between the β-lactam antibiotics and the E-region binding site (pocket 1). Which present a greater number of tunnels and binding interaction surface increasing the probability-based frequency (k-occurrence) in the E-region compared with the two D-regions. However, the energetic contributions based on ΔG repulsive and ΔG rotational forces revealed a similar pattern of interaction with the E-region binding site for both ligands evaluated and were considered with low relevance for the stabilization of the obtained docking complexes from the quantitative point of view in accordance to a non-spontaneous thermodynamic process (ΔG repulsion and ΔG rot > 0 kcal/mol).

Following, we carried out an additional docking simulation in order to identify the individual atom contribution to the total binding affinity (ΔG bind) of each β-lactam antibiotic (ΔG_{bind_Clox} and ΔG_{bind_Diclox}). To this end, a per atom energy contribution analysis was performed regarding the cited thermodynamic energies (ΔG_{Gauss1}, ΔG_{Gauss2}, $\Delta G_{repulsion}$, $\Delta G_{H\text{-}bond}$, $\Delta G_{hydrophobic}$ and $\Delta G_{rotational}$) (**Figures 7; C, D)**. This approach allows a detailed exploration on the contribution of the individual atoms of the β-lactam antibiotic ligands interacting with the fibrinogen E-region binding site (pocket 1) [37, 49,

50]. The results obtained pointing that the docking complex stabilization was mainly based on $\Delta G_{H\text{-}bond}$ interaction atom energy contribution for both ligands evaluated ($\Delta G_{H\text{-}bond\_Clox} > \Delta G_{H\text{-}bond\_Diclox}$). Specifically, we observe that, the maximum atom contribution in the case of cloxacillin was provided by the H-bond interaction, generated by the cloxacillin O-atom-(#1) which belong to the four membered β-lactam ring with an H--O group from the electron-acceptor regulatory residue THR22:P:CA having a maximum atom-energy contribution around -1.4 kcal/mol. While for case of dicloxacillin the H-bond atom contribution occurs in a different position involving the ionized oxygen atom (#1) from the carboxylic group of the thiazolidine-5-membered nitrogen saturated ring with a non-regulatory residue PRO20:P with a lower $\Delta G_{H\text{-}bond}$ atom-energy around -0.5 kcal/mol. Another important difference was identified for the second best-ranked $\Delta G_{H\text{-}bond\_clox}$ atom energy contribution of cloxacillin which involves a H-bond interaction of the oxygen atom (#14) of the β-lactam ring with the regulatory residue THR22:P:CA with energy value ≈ -1 kcal/mol. However, in the case of the oxygen atom (#14) of the dicloxacillin this $\Delta G_{H\text{-}bond\_Diclox}$ atom-energy was negligible with value around -0.2 kcal/mol. Interestingly, we observed an additional $\Delta G_{H\text{-}bond\_Diclox}$ atom-energy contribution involving the oxygen atom (#26) and the nitrogen atom (#30) of the dicloxacillin around -0.45 to -0.35 kcal/mol which are totally absent when we consider the same atom positions (oxygen atom (#26) and the nitrogen atom (#30)) for the cloxacillin molecule. Furthermore, we note the presence of a cluster of hydrophobic C-atoms (#37,#38,#40 and #42) from the dicloxacillin molecules exhibit a higher atom-energy contribution based on the steric Gaussian molecular distance-dependent (Gauss 2_Diclox ≈ -0.38) compared with the energy contribution for the same cloxacillin atom positions with a lower atom-energy contribution (Gauss 2_Clox value ≈ - 0.22 kcal/mol). We suggest that this energetic difference could favors a more efficient pharmacological modulation based on Gauss 2 atom energy contribution (dicloxacillin > cloxacillin) toward to reduce the potential hematotoxicty effects (fibrinolysis) and avoid antibiotic resistance mechanisms.

LPRS maps based on the most relevant interacting E-region chains

By the other hand, we could suggest that the molecular docking mechanism of the evaluated β-lactam antibiotics with the fibrinogen molecule (E-region) is likely-based on local-perturbations (interactions) with regulatory chains (N and Q) of E-region. For this instance, the chains N and Q could be considered like critical targets to establish docking

complexes with high binding affinity with the evaluated β-lactam antibiotics because: i) N and Q chains contain the druggable-regulatory residues (SER50:N and SER50:Q) with high propension to interact with β-lactam antibiotics (refer to **Figure 6**, **B** and **D**), ii) the relative positions for these regulatory residues SER50:N and SER50:Q allow functional conformational changes of E-region. Because, are critically located close to loop-linked to helices (H2 of the Aα and Bβ chains) in the opening of the funnel-shaped hydrophobic cavity (main pocket 1) facing each other in the thrombin binding-domain (**Figure SM3**) and iii) these regulatory residues SER50:N and SER50:Q showed relevant backbone-side-chain acceptor/donor interactions with the pharmacophoric groups (5-membered isoxazolyl ring side-chain) responsible for the biochemical modulation of the β-lactam penicillinase resistance and prevent potential hematotoxicity effects-mediated fibrinolysis for both antibiotic drugs [5]. For this instance, we build the local-perturbation response scanning maps (LPRS maps) for the antibiotic target N and Q chains to model local perturbations induced by the β-lactam antibiotics. It is well-known that the transitions between the E-region functional states (open and close) are dependent on its flexibility properties and require the biophysical and biochemical regulation favored by the network of allosteric communication (inter-residue network communication). LPRS maps approaches are defined from elastic network models (ENM) which offer a computationally attractive way to reduce the dimensionality of the docking problem: do not require time-consuming simulations, benefitting from the high speed and practicality[51-53]. The LPRS maps based ENM models have been widely reported to study relevant conformational changes of several proteins (as fibrinogen) at the atomistic and molecular level. Because, it is well-known that the first elastic normal modes could describe a large number the conformational differences between the protein unbound state (as unoccupied E-region) and the bound state (β-lactam antibiotics interacting with E-region). In this regard, one of the most important steps is the determination of the degree of collectivity of the system evaluated [54, 55]. The degree of collectivity (K_k) of a given mode (k) determines the collective protein motions like an extent to which the structural elements (block of consecutive residues) move together in a given conformational mode. Then, a high degree of collectivity ($K_k \approx 1$) represents a highly cooperative conformational changes strictly dependent on the low-frequency normal modes (k) that exhibit larger amplitudes of correlated motions for a large number of C-(α) atoms affecting partially or the whole structure describing global rotations-translations of consecutive residue blocks by conformational anisotropic movements. While, high-

frequency modes exhibit small amplitude and localized motions (as bending and bond stretching) which are usually associated with low collectivity ($K_k \approx 0$) from residue blocks in the polypeptide chain. In the present work, the anisotropic network models-based on rotations-translations blocks approach (ANM-RTB model [25, 40, 55]) was used because it efficiently provides a good biophysical approach to describe collective motions of atoms as rigid-body translations/rotations of blocks (RTB). Herein, the protein (E-region chains N and Q) was splitted into n-blocks, being a block composed by one or several consecutive residues clustered like rotation-translation-blocks to assess the impact under the absence or presence of docking interactions with the β-lactam antibiotics (cloxacillin and dicloxacillin). To this end, the ANM-RTB models of the interacting N and Q chains were obtained at the low-frequency normal modes as a linear combination of the rotations and translations movements of residue blocks [38]. Specifically, we use the C-(α) atoms of the most relevant interacting E-region chains (N and Q) setting a distance cutoff equal to 10 Å. Then, we perform the energy minimization of the input chains N and Q following the ANM standard procedures. For this instance, all the C-(α) atoms composing the cited chain structures (including the regulatory target residues SER50:N and SER50:Q) were energetically minimized and used to compute the ENM-Hessian matrix. ENM-Hessian matrix allows to evaluate multidimensional potential energy surfaces for biophysical systems (like E-region polypeptide chains N and Q) of coupled C-(α) atoms of residues, where the matrix elements are the second derivatives of the harmonic potential (V). For this instance, for the unbound state for the evaluated receptor chains (R: N and/or Q chains) the Hessian matrix can be defined according to the following general **equation 9**:

$$V_R = \begin{bmatrix} \left(\frac{\partial^2 V_R}{\partial X_i \, \partial X_j}\right) & \left(\frac{\partial^2 V_R}{\partial Y_i \, \partial X_j}\right) & \left(\frac{\partial^2 V_R}{\partial Z_i \, \partial X_j}\right) \\ \left(\frac{\partial^2 V_R}{\partial X_i \, \partial Y_j}\right) & \left(\frac{\partial^2 V_R}{\partial Y_i \, \partial Y_j}\right) & \left(\frac{\partial^2 V_R}{\partial Z_i \, \partial Y_j}\right) \\ \left(\frac{\partial^2 V_R}{\partial X_i \, \partial Z_j}\right) & \left(\frac{\partial^2 V_R}{\partial Y_i \, \partial Z_j}\right) & \left(\frac{\partial^2 V_R}{\partial Z_i \, \partial Z_j}\right) \end{bmatrix} \quad (\mathbf{9})$$

Relevant perturbations which affect the E-region collective motions for the bound state can be also modeled as rigid-body translations/rotations of blocks (RTB) of C-(α) atoms by considering the allosteric signal propagations (local perturbations) released from the critical regulatory-sensor residues (i-residues: SER50:N and SER50:Q) to other consecutive neighboring residues (j-effectors) in the evaluated chain. Herein, the receptor chains (R: N and Q chains) are represented as a projection matrix (P) of an atomistic C-

(α) $3N_a$ x $3N_a$ Hessian matrix (H_b) into a small $6n_B \times 6n_B$ block matrix being given by $H_b = \dot{V}_{(R)_{ij}}^{b} = P^t H P$ [39]. Where, P represents an orthogonal $3N_a$ x $6n_B$ matrix composing by the vectors associated with the local rotation and translation motions-based perturbations of each block (B), N_a represents the number of C-(α) atoms in the evaluated chains (N or Q) with the corresponding number of blocks (n_B) chosen for the evaluated chain in question. Here, the query normal low-frequency modes (k) are the eigenvectors of the cited above Hessian matrix which holds the anisotropic information's on the collective fluctuations of inter-residue network communication observed in crystallographic fibrinogen E-region structure for the N- or C-termini. The $6n_B$ vectors belonging to the projection matrix (P) can be express in a new form as $\dot{V}_{(R-L)_{ij}}^{b} = P_i^t(\dot{V}_{(R-L)_{ij}}^{b})P_j$ for each diagonal block for the bound state. Next, we can rewrite the **equation 9** to study the changes in the conformational dynamic of our systems (chains N and Q) upon docking interaction (bound state) with the ligands (L: penicillin β-lactam antibiotics cloxacillin and dicloxacillin) in the local 3D-space according to the **equation 10**:

$$\dot{V}_{R-L} = \begin{bmatrix} \left(\frac{\partial^2 V_R}{\partial X_i\, \partial X_j} + \frac{\partial^2 V_L}{\partial X_i\, \partial X_j}\right) & \left(\frac{\partial^2 V_R}{\partial Y_i\, \partial X_j} + \frac{\partial^2 V_L}{\partial Y_i\, \partial X_j}\right) & \left(\frac{\partial^2 V_R}{\partial Z_i\, \partial X_j} + \frac{\partial^2 V_L}{\partial Z_i\, \partial X_j}\right) \\ \left(\frac{\partial^2 V_R}{\partial X_i\, \partial Y_j} + \frac{\partial^2 V_L}{\partial X_i\, \partial Y_j}\right) & \left(\frac{\partial^2 V_R}{\partial Y_i\, \partial Y_j} + \frac{\partial^2 V_L}{\partial Y_i\, \partial Y_j}\right) & \left(\frac{\partial^2 V_R}{\partial Z_i\, \partial Y_j} + \frac{\partial^2 V_L}{\partial Z_i\, \partial Y_j}\right) \\ \left(\frac{\partial^2 V_R}{\partial X_i\, \partial Z_j} + \frac{\partial^2 V_L}{\partial X_i\, \partial Z_j}\right) & \left(\frac{\partial^2 V_R}{\partial Y_i\, \partial Z_j} + \frac{\partial^2 V_L}{\partial Y_i\, \partial Z_j}\right) & \left(\frac{\partial^2 V_R}{\partial Z_i\, \partial Z_j} + \frac{\partial^2 V_L}{\partial Z_i\, \partial Z_j}\right) \end{bmatrix} \quad (\mathbf{10})$$

In this context, for calculating the normal modes we use Dynomics software (DIAGQ routine) [56]. Which automatically allows the diagonalization of the obtained ENM-Hessian matrix for the minimized unbound chain structures (by diagonalizing the N and/or Q Hessian matrix) and in the presence of β-lactam antibiotics by diagonalizing the receptor–ligand docking complexes (R-L Hessian matrices) namely: chain N+cloxacillin, chain N+dicloxacillin, chain Q+cloxacillin, chain Q+dicloxacillin, chain N-Q+cloxacillin, chain N-Q+dicloxacillin, considering in all the cases, the best crystallographic docking poses. Then, we tackle the construction of the local perturbation response scanning maps (LPRS maps) based on the low-frequency modes (k) [57]. The LPRS maps generates a comprehensive visualizations which allows evaluate allosteric signal propagations in response to external perturbations (i.e., as induced by the β-lactam

antibiotic interactions from the regulatory residues SER50:N and SER50:Q). Following this idea, we suggest that conformational changes in the intrinsic chain dynamics, as well as, perturbations in the flexibility properties of the N and Q chains could be associated to potential side effects of cloxacillin > dicloxacillin as anomalous binding of the thrombin molecule in the E-region due to loss of allosteric cooperative mechanisms and conformational coupling between normal modes (degree of collectivity) for these target chains under β-lactam antibiotic docking interactions. The degree of collectivity (K_k) for a given block of consecutive residues is proportional to the exponential of the ‘‘information entropy’’ of the eigenvector (k-mode) and can be defined according to Bruschwiler's **equation 11**:

$$\text{Collectivity\_K}_k = \frac{1}{N}\exp\left(-\sum_i^N \alpha\left(\Delta d_{ij\_k}\right)^2 \log\alpha\left(\Delta d_{ij\_k}\right)^2\right) \qquad (\mathbf{11})$$

where, are included the sum of all N atoms of the molecule (fibrinogen E-region chains), the term d_{ij_k} represents the amplitude of the displacement of the atom i in the elastic normal mode k, and α is a normalization parameter which correspond to $\sum_i^N \alpha\left(\Delta d_{ij\_k}\right)^2 = 1$. Herein, $\Delta d_{ij\_k} = d_{ij\_k} - d^0_{ij\_k}$ which represents the displacement for different amplitudes between the unperturbed and the perturbed state of the displacements (distance-based local perturbations) from equilibrium represented by ($d^0_{ij\_k}$). According to this, we could represent the degree of collectivity for locally perturbed fibrinogen chains (R, receptor as N and Q chains) interacting with the β-lactam antibiotics (L, ligands as cloxacillin or dicloxacillin) by replacing the terms in the Bruschwiler's **equation 12**.

$$\text{Collectivity\_K}_{k(R-L)} = \frac{1}{N}\exp\left(-\sum_{i=1}^{N=7} \alpha(d_{R-L} - d^0_R)^2 \log\alpha\,(d_{R-L} - d^0_R)^2\right) \qquad (\mathbf{12})$$

herein, the low-frequency normal modes allow to efficiently characterize the collective motions of the relevant receptor chains N and Q which are directly associated to functional conformational changes of E-region (main pocket 1). To address the evaluation of the corresponding (3N)-XYZ-atomic displacements we use the $d_{ij}(d^0_{ij})$ which represent the distance between the conformational dynamical in equilibrium of the C-(α) atoms network using a d_{cutoff} = 7 Å which allows map the conformational response triggered from the i-sensor regulatory residues (SER50:N and SER50:Q) to j-effector

residues. In this context, the displacement vector in the (3N)-XYZ-Cartesian representation can be extracted from the aforementioned equations to represent distance-based perturbations for the evaluated conformational states (unbound and bound) for the interacting N and Q chains as:

$$\Delta d_{ij\_k} = (X_1 - X_1^0, Y_1 - Y_1^0, Z_1 - Z_1^0, \ldots X_N - X_N^0, Y_N - Y_N^0, Z_N - Z_N^0)^t \quad (\mathbf{13})$$

Next, the **equation 9** can be rewritten as:

$$V_R = \sum_{(i<j)\in N(R)} \frac{1}{2} \gamma_R \left(\Delta d_{ij\_k}\right)^t \left(\Delta d_{ij\_k}\right) \quad (\mathbf{14})$$

By the other hand, in the present study we rigorously set the degree of collectivity for the first seven low-frequency normal modes (k, from 1 to 7, see **Figure SM4**). It is important to highlight that the linear combinations of normal mode eigenvectors are defined by their correlation to the van der Waals forces derived from each C-(α) atom. Which as mentioned above, are heterogeneously distributed across the overall E-region structure in the inter-residue network that form the cluster of hydrophobic sub-cavities in the fibrinogen E-region. To explore conformational changes of regulatory chains (N and Q) under the presence of β-lactam antibiotics inducing local perturbations we perform the LPRS maps in collective low-frequency modes (K_k, from 1 to 7). See **Figures 8** and **9**.

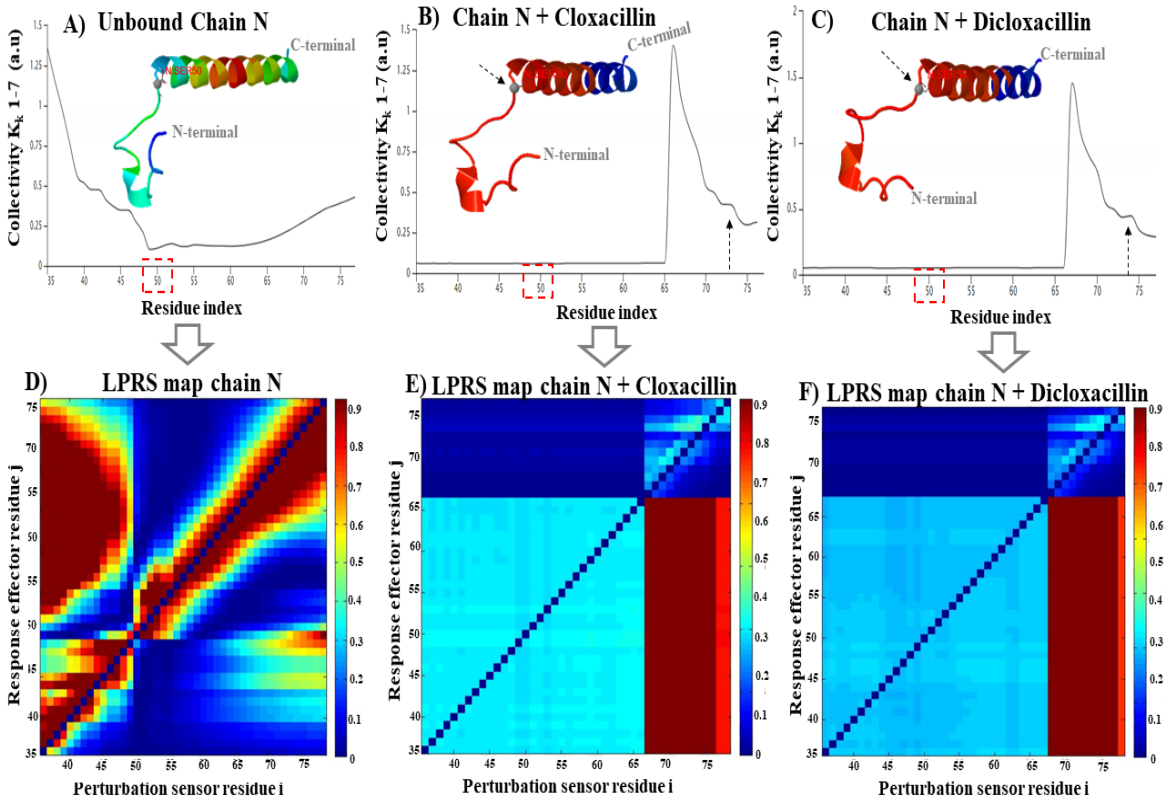

Figure 8. On the top, graphical representation of the behavior of the parameter degree of collectivity K_k (a.u) for the first seven low frequency normal modes 1-7 vs. chain N residue index, highlighting the local perturbations from the regulatory residue SER50:N (red dashed-line rectangle) under different simulation conditions as **A)** unbound chain N, **B)** chain N + cloxacillin, and **C)** chain N + dicloxacillin. The dotted black arrows represent long distance-based perturbations from the regulatory residue SER50: N. On the bottom, graphical representations of the generated local perturbation response (LPRS maps) showing the relationship between (i-j)-pairs of residues as i-sensor residues (x-axis) to j-effector residues (y-ordinates) depicted like a 2D-matrix of allosteric network communication of inter-residue (i-j pairs as off-diagonal elements) and intra-residue (i-i pairs diagonal elements). On the far right of each LPRS map, the bar-color from blue to yellow regions correspond to weak to moderate local perturbations in the inter-residue communication for (i-j)-pairs of residues, and the orange to dark red regions represent strong inter-residue local perturbations for the aforementioned simulation conditions as **D)** unbound chain N, **E)** chain N + cloxacillin, and **F)** chain N + dicloxacillin.

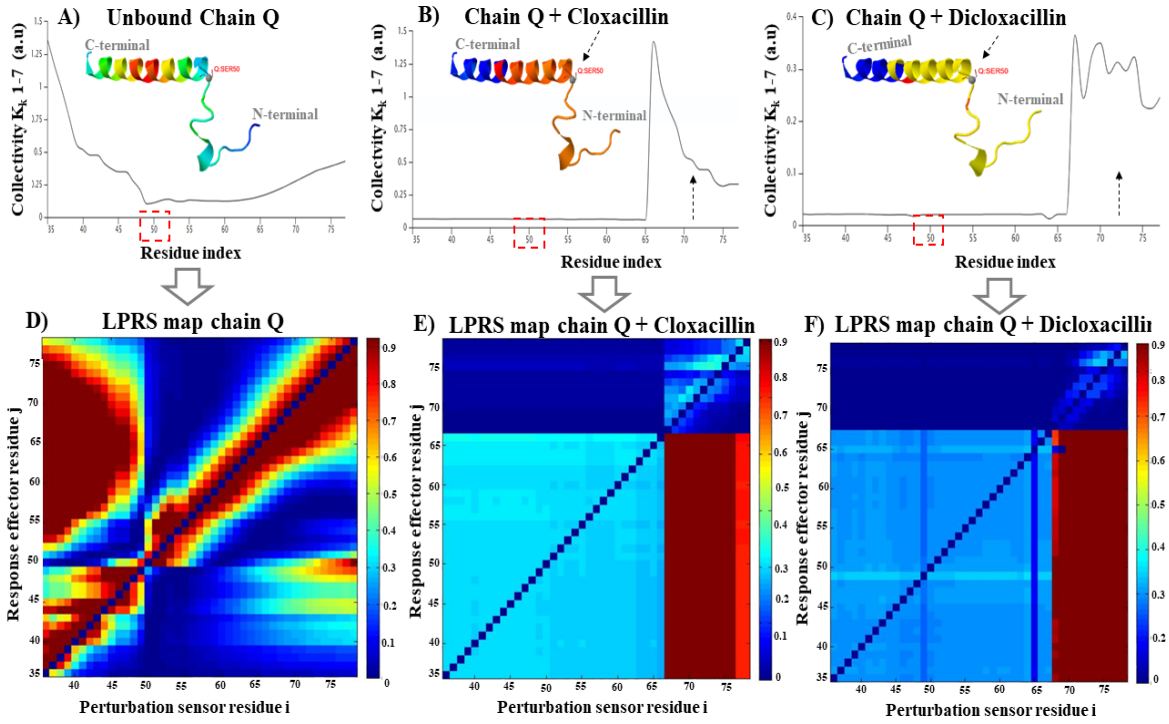

Figure 9. On the top, graphical representation of the behavior of the parameter degree of collectivity K_k (a.u) for the first seven low frequency normal modes 1-7 vs. chain Q residue index, highlighting the local perturbations from the regulatory residue SER50:Q (red dashed-line rectangle) under different simulation conditions as **A)** unbound chain Q, **B)** chain Q +cloxacillin, and **C)** chain Q + dicloxacillin. The dotted black arrows represent long distance-based perturbations from the regulatory residue SER50: Q. On the bottom, graphical representations of the generated local perturbation response (LPRS maps) showing the relationship between (i-j)-pairs of residues as i-sensor residues (x-axis) to j-effector residues (y-ordinates) depicted like a 2D-matrix of allosteric network communication of inter-residue (i-j pairs as off-diagonal elements) and intra-residue (i-i pairs diagonal elements). On the far right of each LPRS map, the bar-color from blue to yellow regions correspond to weak to moderate local perturbations in the inter-residue communication for (i-j)-pairs of residues, and the orange to dark red regions represent strong inter-residue local perturbations for the aforementioned simulation conditions as **D)** unbound chain Q, **E)** chain Q + cloxacillin, and **F)** chain Q + dicloxacillin.

The results on LPRS maps allowed us to investigate the collectivity parameters in low-frequency modes (k, from 1 to 7), and explain the observed larger-scale movements associated to long distance-based allosteric signal propagation affecting the inter-residue

network communication. In this concern, the degree of collectivity and LPRS maps pointing clearly that both antibiotics cloxacillin and dicloxacillin can significantly affect the intrinsic dynamics of the relevant regulatory chains (N and Q) that form part of the fibrinogen E-region (main pocket 1) by reducing the K_k-values when we compare the unbound state (as reference control of simulation) with the bound state, for both chains. See **Figure SM5.** Although, the evaluated antibiotics belong to the same pharmacological group exhibit a different docking interaction mechanism without significantly compromising the binding affinity values (- 0.1 kcal/mol of variation between both). In this sense, we theoretically show that the cloxacillin and dicloxacillin could significantly affect (i.e., induce conformational perturbations) in a large blocks of neighboring residues from both polypeptide chains when the regulatory i-sensor residues SER50:N and SER50:Q are perturbed by the β-lactam antibiotics interaction (i.e., signal propagation generated from SER50:N and SER50:Q in both, N-terminal and C-terminal direction from the regulatory chains N and Q). Specifically, around 31 consecutive amino acid residues were conformationally perturbed with an abrupt decrease in the degree of collectivity in the C-terminal direction (See **Figure 8B**,**C** and **Figure 9B**,**C**) from GLY35:N to regulatory non-target THR65:N and from GLY35:Q to regulatory non-target THR65:Q. Consistent with phenomena of conformational rigidification in large cluster of residues according to the results of the corresponding LPRS maps (regions colored from light blue to dark blue) as showed in the **Figure 8E**,**F** and **Figure 9E**,**F** for the chains N and Q, respectively. The conformational rigidification in both chains (N and Q) in the bounded state is remarkable when we compare with the reference control represented by the unbound state for the chains N and Q as unperturbed crystallographic native conformation (including the unbound residues SER50:N and SER50:Q). See **Figure 8A**, **D** and **Figure 9 A**, **D**.

As mentioned above, a significant decrease in the degree of collectivity of the chains for K_k-values ≈ 0 is frequently associated to localized vibrational motions of a few atoms. Therefore, we strongly suggest that the β-lactam antibiotic docking interaction could induce several local perturbations based on bending and bond stretching in the inter-residue network for the target chains N and Q and theoretically promoting a significant rigidification associated to perturbation in the flexibility properties of this chains following the order (chain N + dicloxacillin > chain N + cloxacillin >> chain N) and (chain Q + dicloxacillin > chain Q + cloxacillin >> chain Q). Apparently, a transient

decrease of the degree of collectivity in the first block of residues composing the unbound state of the chains N and Q (ranging from the GLY35 to regulatory non-target THR65 residue index positions in both chains, N and Q); favor the correct accommodation and required adjustment of the native substrates (thrombin) in the E-region (pocket 1) during the coagulation process. However, from the pharmacological point of view, the potential docking interactions as promoted by parenterally administrated β-lactam antibiotic with the fibrinogen blood plasma protein, could theoretically affect the binding of thrombin associated with a significant decrease of the degree of collectivity with K_k-values ≈ 0, in these block of residues; leading appreciable changes in the conformational architecture of the E-region inter-residue network communication in the bound state generated from distance-based local perturbations initiated in SER50:N and SER50:Q. Leading potential hematotoxicity (fibrinolysis), which as mentioned above, is considered as one of the most severe adverse reactions induced by penicillin β-lactam antibiotics when are parenterally administrated [5]. In addition, we observed that both antibiotics cloxacillin and dicloxacillin promote a significant increase in the degree of collectivity with a peak, and subsequently an abrupt decrease of the collectivity parameter (K_k-values) in the residue range from Phe 65:N to SER 75:N, with subtle conformational differences as can be observed in the end of the profiles of collectivity mode vs. residue index. Where, dotted black arrows representing long distance-based perturbations (**Figure 8**, **B** and **C**) and in the corresponding LPRS maps (**Figure 8**, **E** and **F**). Where, a strong local perturbations were observed for the docking complexes formed by chain N + cloxacillin ≈ chain N + dicloxacillin involving the signal transduction of the perturbations from the block of i-sensor residues (from regulatory non-target SER67:N to Phe79:N) which trigger strong allosteric responses in the j-effector residues (ranging from GLY35:N to regulatory non-target THR65:N). Herein, non-target regulatory residues (SER and THR) are referred to residues which do not directly interact with antibiotics evaluated. By the other hand, when both antibiotics interact with the chain Q (**Figure 9**, **B** and **C**). Just the cloxacillin keeps the same pattern of K_k-value perturbation previously observed for the interaction with the N chain. However, when the regulatory target SER50:Q is perturbed by the dicloxacillin ligand the chain Q exhibit a different pattern of signal propagation across its inter-residue network communication involving the appearance of several peaks or fluctuations of the K_k-values compared with the simulation condition for the chain Q for the complex formed by the Q-chain+cloxacillin, where the aforementioned fluctuation as peaks of the K_k-values were not observed in the residue range from PHE65:N to SER 75:N (**Figure 9**, **B**

and **C**). More details can be found in **Figure SM5**. Furthermore, the obtained LPRS maps for the docking complexes formed by chain Q + cloxacillin and chain Q + dicloxacillin exhibit slight differences in the pattern of signal propagation of the chain Q inter-residue network under interactions with the cited antibiotics (**Figure 9**, **E** and **F**). In this regard, we note the presence of greater number of long-distance-based local perturbations following the order: chain Q + dicloxacillin > chain Q + cloxacillin >> chain Q. Particularly, involving the signal transduction-based perturbations from the block of i-sensor residues (from regulatory non-target SER67:Q to PHE79:Q) triggering allosteric responses in j-effector residues (ranging from GLY35:Q to PHE79:Q). This, fact could be associated to the different crystallographic docking pose orientation of the CL-atom(s) of the dicloxacillin respect to cloxacillin during the interactions with E-region as previously showed 3D-lig-plot analysis **(Figure 6**). Please, also refer to **Figure SM1** and **Figure SM2**. To validate the intrinsic conformational dynamic of the target N and Q chains evaluated. The Ramachandran analysis was carried up as a control test to avoid obtain false positives from the results of the LPRS maps. Also the Ramachandran plots obtained from the individual regulatory residues SER50:N and SER50:Q were considered. See **Figure SM6**. In this regard, allowed torsion values for *Phi vs. Psi* dihedral angles were unequivocally identified inside the Ramachandran colored purple contour lines in both chains (*i.e.,* conformationally-favored N and Q chains including their corresponding regulatory E-region residues SER50:N and SER50:Q). Corroborating that overall results obtained from the LPRS maps were carried out in the total absence of sterically disallowed residues which are usually associated with torsion dihedral angles Psi vs. Phi values ocurring outside of the Ramachandran colored purple contour lines. These results are the paramount importance because it is well known that (C···C)-backbone-side-chain interactions (bound state) are associated to fluctuations of adjacent dihedral angles Psi and Phi through collective angular motions. **REF55**

Besides, we carried out additional simulations by considering the LPRS-maps and 2D-matrix cross-correlation of flexibility for both interacting chains (N and Q) in the bound state and the showing that the cloxacillin and dicloxacillin can modulate the signal allosteric propagations and flexibility properties of the inter-residue network composing the E-region. See **Figure SM7** and **Figure SM8**.

It is important to note that, in order to validate our ANM results we perform control simulation experiments by applying well established normal mode approaches based on several DynaMut-ANM force fields namely: i) C-(α) force field derived from

Amber94 all-atom potential, ii) ANM simplified spring force constant-based pair-wise distance, iii) pfANM parameter-free ANM as alternative from the ANM force field with perturbations which fall off with the square of the inter-residue distance, iv) REACH called realistic extension algorithm-based covariance Hessian parameterized with variance-covariance matrices, and lastly sdENM which employs residue-specific spring force constants based on parameterized statistical analysis of > 1500 NMR-ANM molecular ensembles [58, 59]. These control ANM-validation procedures fit well with our ANM results (i.e., getting similar K_k-values for the evaluated N and Q fibrinogen E-region chains) corroborating that the proposed ANM models are robust, and can be efficiently applied to evaluate the conformational properties of our systems under the unbound and bound states with the penicillin β-lactam antibiotics.

Experimental section

To determine accurate thermodynamic parameters of fibrinogen-cloxacillin and fibrinogen-dicloxacillin interactions, ITC measurements were conducted. Representative calorimetric titration profiles of the binding of both systems are show in **Figure 10**. The titration results in negative heat deflection indicating that the reactions are exothermic in nature which shows that binding is the predominant reaction, while conformational changes of fibrinogen, if any, barely leave an energy footprint (endothermal peaks) in the graphs. It is also relevant to comment on the different patterns followed by both binding processes. While cloxacillin shows a more abrupt process characterized by sigmoid-type function, the interaction of dicloxacillin with fibrinogen has a smoother profile represented by a decreasing exponential function. That is, while dicloxacillin interacts immediately and constantly with fibrinogen, cloxacillin needs a threshold concentration, above which the interaction is more favorable, and the protein is saturated earlier. In the molecular docking section (refer to **Figure 6**), we pointed out that once adsorbed both β-lactam antibiotics adopt a different crystallographic binding conformation (i.e., cloxacillin more extended and dicloxacillin more closed). This ability to adapt to the pocket makes the adsorption process of dicloxacillin easier and more gradual. While in the case of the cloxacillin, its greater rigidity makes the pocket needs to adapt previously to later interact more abruptly.

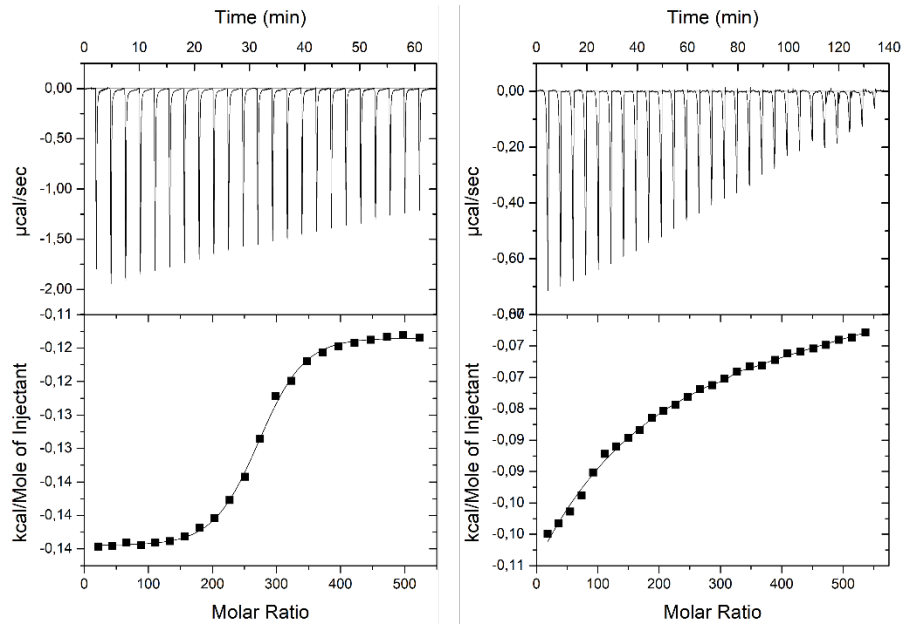

Figure 10. ITC profiles for the binding of cloxacillin (left) and dicloxacillin (right) to fibrinogen.

Table 1. Thermodynamic parameters: binding constant (***K***), enthalpy (**Δ*H***), entropy (***T*Δ*S***) and free energy (**Δ*G***) of binding of cloxacillin and dicloxacillin with fibrinogen according to a single binding site

	***K*(M^{-1})**	**Δ*H*(kcal mol^{-1})**	***T*Δ*S* (kcal mol^{-1})**	**Δ*G* (kcal mol^{-1})**
Cloxacillin	6.9×10^3	-13.1	-4.5	-8.6
Dicloxacillin	6.5×10^3	-11.4	-5.3	-6.1

Fits of a standard non-linear least-squares regression binding model to the ITC measurements revealed that both penicillin β-lactam antibiotics bind to fibrinogen binding site at a 1:1 molar ratio, corroborating the computational results that predicted a single adsorption in the E-region binding site (main pocket 1). The corresponding thermodynamic parameters are listed in **Table 1**. The values of the binding constants are of the order of 10^3, suggesting that both β-lactam antibiotics are moderate binders. As summarized in the **Table 1**, thermodynamic parameters show a common pattern for the two evaluated penicillins, although they differ in their numerical values. Hydrogen bond, hydrophobic force, and electrostatic interaction mainly contributed to the interactions between proteins and ligands. The obtained enthalpy and entropy values are negatives. Referring to enthalpy, this means that the binding is driven by the formation of non-covalent bonds (hydrogen bond, electrostatics, π-π interactions). The fraction of non-

ionized molecules of cloxacillin and dicloxacillin at pHs 8.5, the carboxyl group is not dissociated, is around 5.5% [60]. This means that some of the molecules are neutral which prevents their electrostatic interaction with fibrinogen, resulting in a decrease in the value of enthalpy. For this reason, within the interactions that we have just pointed out as responsible for the bonding process, hydrogen bonds are the dominant. These experimental facts reinforce the theoretical results that underline the important role of Gauss 2 forces in these interactions. In the case of negative entropy change, it reveals hydration and a loss of conformational freedom associated with the complex formation. Bearing in mind the similarities between binding and β-lactam antibiotic self-aggregation process [10], we can conclude that desolvation is not present in this binding process as entropy has already been pointed out. So, changes in translational and rotational degrees of freedom, alterations of the conformational flexibility of the binding partners, and reorganization of solvation shells upon binding become the main contributions to entropy change. Comparison of values for cloxacillin and dicloxacillin shows that the former drug has more negative enthalpy values and higher affinity constant. These differences arise from the existence of a second Cl atom in a meta position to the first in dicloxacillin if compared to cloxacillin. Halogen bonding has been widely documented in supramolecular systems; specially for its possible role in the stabilization of small ligand–protein complexes. It is also shown that aromatic halogen substitutions affect the optimal geometries and σ-hole characteristics of the formed complexes, often as the result of secondary interactions [61, 62]. Memic et al. found that binding thermodynamic parameters are perturbed when the position and identity of halogen substituents are varied, in fact, they obtained an increase in entropy and a decrease in enthalpy when interactions take place in a single binding pocket[63]. In view of the experimental and computational results, associated to the effect of the second Cl atom, the conformational changes that cloxacillin undergoes must also be considered as the origin of the differences in thermodynamic magnitudes.

With a view to completing the energy landscape of these binding processes we have used DSC measurements. The DSC thermograms from pure fibrinogen and in the penicillin β-lactam antibiotics containing solutions are shown in **Figure 11**. The three endothermic peaks at 52, 76 and 93 ºC have been attributed to the denaturation of the D, C and E domains of the fibrinogen molecule. Due to the intensity and relevance of the two largest peaks, we will focus only on them, calling peak 1 and peak 3 respectively. The thermodynamic characteristics of the thermal denaturation, melting temperatures

(T_m, temperatures at which a maximum occurred in the endothermic peaks), calorimetric enthalpy (ΔH), van't Hoff enthalpy (ΔH_v), and cooperativity (n, the ratio of calorimetric enthalpy to van't Hoff enthalpy) were obtained for all the systems studied and listed in **Table 2**.

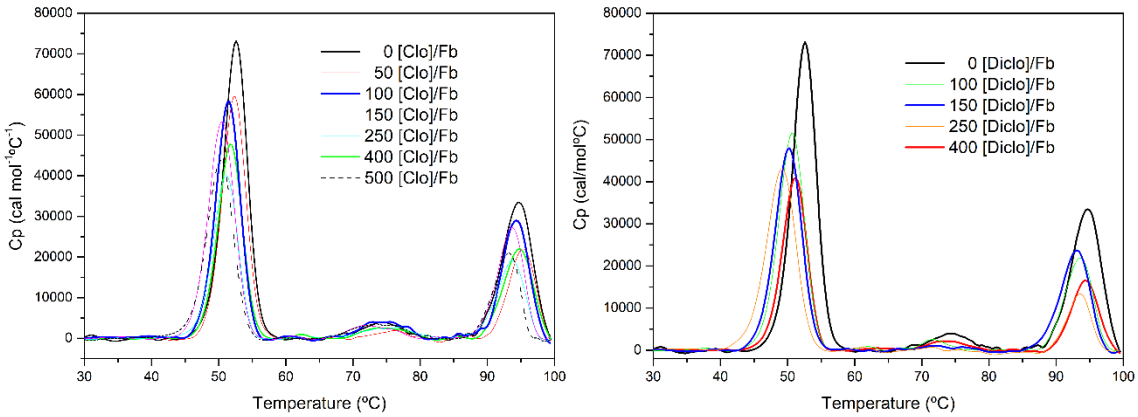

Figure 11. DSC thermograms of fibrinogen in the presence of different concentrations of cloxacillin (left) and dicloxacillin (right).

As can be seen in **Figure 11**, as the concentration of the β-lactam antibiotics increases, the area of the endothermic peaks decreases, and they move towards lower temperatures or disappear as in the case of the second peak with respect to pure fibrinogen. Significant changes in peak characteristics are induced by higher penicillin concentrations. This first set of measurements points out a decrease in stability of fibrinogen with increase in the β-lactam antibiotic concentration. Such a fact has been previously observed in other systems[64]. Concerning cooperativity, n (the ratio between van't Hoff and calorimetric enthalpies) when $n > 1$, the unfolding is not a two-state process but involves unfolded intermediates states. In the case of $n < 1$, this implies that the overall protein is not correctly folded. For all studied systems the values we have obtained are slightly higher that the unit. Theoretically, this implies that one or more intermediate states are populated in the temperature change[65] , however, in a previous paper and based on SAXS measurements we demonstrated that in fibrinogen solutions coexists two species, the monomeric molecule (63 %) and a dimeric complex (37%) [66]. Therefore, we associate the values of cooperativity we have obtained with the presence of the two species that alter the hypothesis of a two-state process.

Table 2. Thermodynamic parameters obtained from DSC thermograms in the presence of cloxacillin and dicloxacillin.

Cloxacillin							
ratio	T_{m1} (ºC)	T_{m3} (ºC)	ΔH_1 (cal mol^{-1})	ΔH_3 (cal mol^{-1})	ΔH_{v1} (cal mol^{-1})	ΔH_{v3} (cal mol^{-1})	n
0	52.4	94.4	3.34×10^5	1.92×10^5	1.88×10^5	2.28×10^5	1.78
50	52.2	95.1	2.72×10^5	1.47×10^5	1.87×10^5	2.27×10^5	1.44
100	51.7	94.5	2.69×10^5	1.35×10^5	1.84×10^5	2.24×10^5	1.20
150	51.3	94.1	2.65×10^5	1.23×10^5	1.85×10^5	2.20×10^5	1.45
250	51.0	93.4	2.22×10^5	1.10×10^5	1.82×10^5	2.11×10^5	1.03
400	50.3	93.4	1.88×10^5	1.01×10^5	1.71×10^5	2.01×10^5	1.55
500	50.1	92.8	1.67×10^5	0.99×10^5	1.67×10^5	1.95×10^5	1.00
Dicloxacillin							
0	52.4	94.4	3.34×10^5	1.92×10^5	1.87×10^5	2.54×10^5	1.78
100	51.0	94.2	2.54×10^5	1.29×10^5	1.81×10^5	2.18×10^5	1.06
150	50.5	93.3	2.44×10^5	1.15×10^5	1.72×10^5	2.10×10^5	1.42
250	50.1	92.8	2.41×10^5	0.84×10^5	1.66×10^5	1.99×10^5	1.46
400	49.0	93.3	1.93×10^5	0.60×10^5	1.49×10^5	1.98×10^5	1.61

The data shown in the **Table 2** can give us useful information about the effect of these drugs on fibrinogen stability. If we extrapolate the enthalpy values obtained for both peaks to null β-lactam antibiotic values, we obtain: 291 and 143 kcal mol^{-1} for cloxacillin and 273 and 149 kcal mol^{-1} for dicloxacillin (first and third peak, respectively). The total enthalpy of unfolding will be sum of both peaks. These extrapolated values could be interpreted as the protein denaturation enthalpy in the absence of drug. However, they values are different. Even if we assume the thermal unfolding of fibrinogen in the presence of the drugs in two stages: first the drugs are bound to the native protein (binding energy from ITC) and then the complex is denatured (DSC). The sum of both enthalpies, binding and extrapolated, do not match the value of denaturation of pure fibrinogen. These energy differences, 92 and 201 kcal mol^{-1} for cloxacillin and dicloxacillin, serve to quantify the effect that β-lactam antibiotics have on the stability of the fibrinogen molecule. Thus, dicloxacillin has a much more destabilizing effect on the fibrinogen molecule. These quantitative measurements are perfectly consistent with the LPRS maps that suggested that the process of penicillin β-lactam antibiotic adsorption involved allosteric signal perturbations in the fibrinogen molecule that were transmitted through

the N and Q chains, these perturbations being greater for dicloxacillin. Demonstrating in this way how the combination of ITC and CRP measures provide information on change in protein conformational flexibility see **Figure 13** and refer to **Figure SM8** for more details.

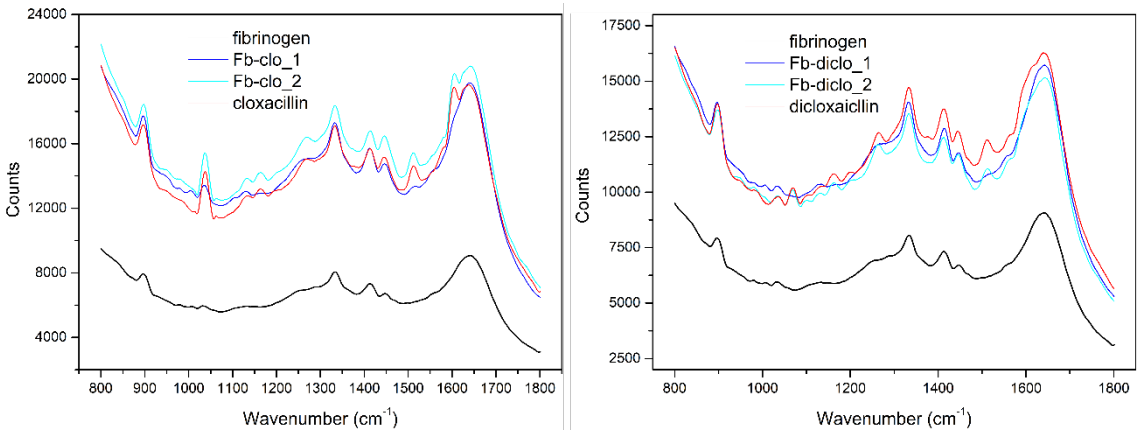

Figure 13. Raman spectra of fibrinogen in presence of different penicillin ratios, 100 and 400 for samples 1 and 2 respectively.

In order to understand how drugs, affect the secondary structure of the protein, we have analyzed Raman spectra for fibrinogen in the presence of both penicillins at two different ratios, see **Figure 13**. The amide I band, between 1600 cm^{-1} and 1700 cm^{-1} is stronger than the Amide III band and is composed by the contributions of α-helix at 1655 cm^{-1}, β-sheet at 1670 cm^{-1} and random coil at 1680 cm^{-1}. Other small peaks are attributed to: C_α-C stretch (895 cm^{-1}), PHE and TRP (1035 cm^{-1}), Amide II (1328 cm^{-1}), N-H bend indole ring (1414 cm^{-1}), C-H_2 and CH_3 deformation (1448 cm^{-1}) and TRP (1554 cm^{-1}) [67]. In the presence of penicillin, amide I band shifts to lower wavenumbers. These changes in the position (and intensity) of the amide I band indicate that under drug interactions the fibrinogen experiment changes in the secondary structure mainly in the α-helix content and with more intensity in the case of cloxacillin. Considering that the modifications in the spectrum occur mainly in this area, it can be postulated that the adsorption occurs in lateral chains of amino acids (N and Q chains, as suggested by the LPRS maps), altering the contents of secondary structure but with few changes in the general structure of the protein.

Figure 14 shows the effect of cloxacillin and dicloxacillin on fluorescence emission spectra of fibrinogen at two temperatures. The absorption peak of the fibrinogen

alone can be found at about 350 nm at the excitation wavelength of 280 nm. Both drugs have a similar effect, as the concentration of the drugs was increased the fluorescence emission intensity decreased regularly. It has been reported that those changes in fluorescence are correlated with the number of cleaved disulfide bonds upon irradiation and the reduction of the disulfide bond makes the fluorescence intensity higher. Consequently, the interaction of the penicillin β-lactam antibiotics with fibrinogen causes the raise in the polarity of fibrinogen fluorophore surrounding. The fluorophore involves the presence of aromatic residues such as tyrosine and tryptophan since they emit fluorescence at the excitation wavelength of 280 nm. The reduction of the maximum peak suggest that the aromatic residues present on the samples had its surrounding environment modified, eventually being more hydrophilic with the increase of the drugs in the solution. Both penicillin β-lactam antibiotics follow similar patterns with concentration and temperature; however, the quenching effect of dicloxacillin is the highest and increases with temperature. Since interaction have to occur in the pocket at E-domain and in view of the computational results, we identified the allosteric residues PHE79:N, PHE65:N and PHE79:Q as the main responsible for this shift due to changes in their biophysical environment. Considering that the binding sites were independent and non-interactive, the Stern-Volmer's equation was used to study and analyze further the intrinsic quenching fluorescence:

$$\frac{F_0}{F} = 1 + K_{sv}[penicillin] \quad \textbf{(15)}$$

F_0 and F are the fluorescence emission intensities with the presence or without the presence of penicillin β-lactam antibiotics, [penicillin] is the concentration of cloxacillin (or dicloxacillin) and K_{sv} the Stern-Volmer quenching constant.

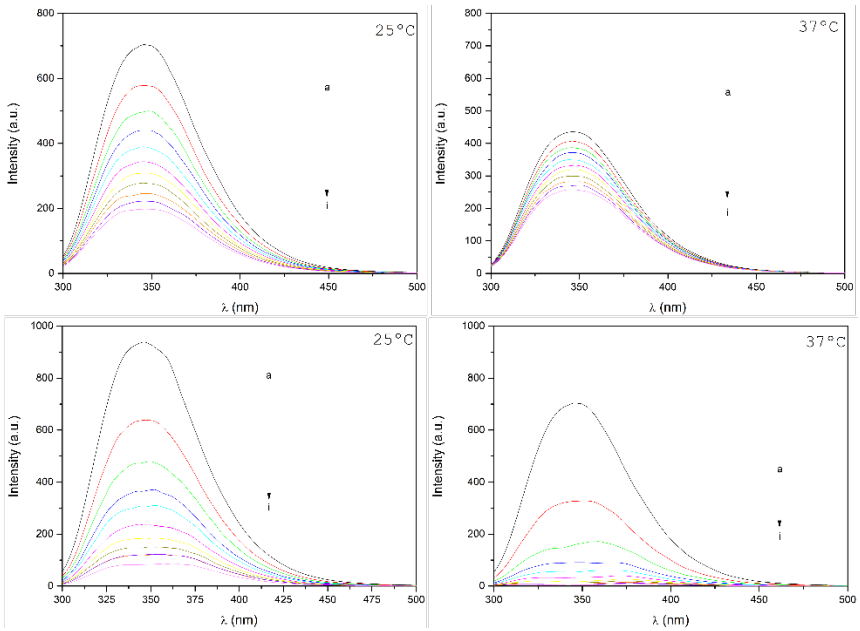

Figure 14. Fluorescence emission spectra of Fibrinogen at two temperatures in the absence and presence of cloxacillin (up) and dicloxacillin (down). Fibrinogen concentration: (a-i) = 1 μM. Cloxacillin concentrations: (a-i) = (0, 0.3, 0.7, 1, 1.3, 1.7, 2, 2.3, 2.7, 3, 3.3 μM). Dicloxacillin concentrations: (a-i) = (0.08, 0.17, 0.25, 0.33, 0.42, 0.5, 0.58, 0.66, 0.75, 0.83 μM).

According to the Stem-Volmer's equation, the linearity of F_0/F vs. the drug concentration, [β-lactam antibiotic], reveals the quenching type. In this system, linear correlations were probed at different temperatures with different values of R coefficient, meaning that all TRP(s) amino acid residues present in macromolecule differ slightly in accessibility[68]. The slope of the straight line gives the K_{sv} values: 43.1 and 18.4 x 10^3 L mol^{-1} at 25 ºC and 37 ºC, respectively for cloxacillin. The obtained values for dicloxacillin were: 59.6 and 152 x 10^3 L mol^{-1} at 25 ºC and 37 ºC. Since the fluorescence lifetime of the fibrinogen in water is 10^{-8} s^{-1} and considering that: $K_q = K_{sv}/\tau_0$, the K_q can be obtained. Bearing in mind that the maximal dynamic quenching constant of the fibrinogen 2.0 x 10^{10} L M^{-1} s^{-1}, so all our values of K_q for both β-lactam antibiotics and temperatures are higher, so in these cases is safe to assure that the quenching of fibrinogen by cloxacillin and dicloxacillin is not initiated by dynamic collision but from the formation of a complex [69].

Fluorescent measurements are also a great tool to get quantitative information about the static quenching process. The binding constant (K_a) and the number of binding sites (n) can be obtained using the following **equation 16**:

$$lg\frac{(F_0-F)}{F} = lgK_a + n \cdot lg[penicillin] \quad \textbf{(16)}$$

The slope of the linear plot of log [(F_0–F)/F] as a function of $lg[penicillin]$ gives the binding sites, while the binding constant can be obtained from the intercept. In the present case, the values of n and K_a were 1.06 and 1.55×10^3 M^{-1} and 1.09 and 1.02×10^3 M^{-1} for cloxacillin at 25 and 37 ºC, respectively. In the case of dicloxacillin the values were 0.94 and 1.79×10^3 M^{-1} and 1.13 and 1.81×10^3 M^{-1} at 25 and 37 ºC, respectively. Clearly, the results indicate that the complexation of fibrinogen with both β-lactam antibiotics are very similar: they interact in one independent class of binding sites, forming a 1:1 complex, as all other experimental and computational approaches have indicated.

Conclusions

In the present study we combined computational and experimental approaches to evaluates the conformational binding mechanisms of fibrinogen under interaction with recognized β-lactam antibiotics. The computational results pointing that despite these conformational differences, both antibiotics exhibit very similar affinity-based on the obtained free binding energy values. Besides, the semi-synthetic incorporation of an additional halogen Cl-atom in the dicloxacillin molecule respect to cloxacillin molecule, and its relative docking-pose orientation in the fibrinogen E-region could significantly reduce the appearance of potential fibrinolytic side-effects affecting the clotting process which are usually associated to β-lactam antibiotic parenterally administered. The performed 3D/2D-lig-plot diagrams revealed that the most relevant antibiotic interactions with the E-region (pocket 1) are mainly based on hydrophobic (C···C)-backbone-side-chain non-covalent and acceptor/donor interactions with critical regulatory E-region residues (SER50:Q > SER50:N) with high H-bond atom energy contribution required for the docking complex stabilization for both drugs. Besides, collective low-frequency normal modes and LPRS maps revealed the subtle differences in the conformational dynamics of relevant E-region chains under unbound and bound state with the β-lactam

antibiotics. Next, we strongly suggest that the differences in the conformational binding mechanism for dicloxacillin and cloxacillin, predominantly involve the allosteric modulation, long-distance perturbations, and remarkable conformational rigidification of the regulatory chains from E-region (N and Q). The experimental results excellently corroborated the computational predictions from: stoichiometry, target-residues, and binding energies. Also, the relevant role that the penicillin molecular structure play in the binding process was confirmed by quantitative calorimetric data on ITC and DSC allowed us to quantify energetically the role played by the elasticity of fibrinogen.

Finally, the obtained results are the paramount importance during the "*de novo rational drug-design"* of new derivatives of β-lactam antibiotics to avoid potential fibrinolytic side-effects, increase the target selectivity/specificity with optimal benefit/risk rates beyond the β-lactam antibiotic drug resistance phenomena, and favor the implementation of rigorous criteria for a more personalized antibiotic therapy.

Acknowledgements

The authors acknowledge Ministerio de Ciencia e Innovación (PID2019-111327GB-100) and Xunta de Galicia (ED41E2018/08). Also, M. G.-Durruthy acknowledge the FCT/MCTES national funds.

References

[1] N. Vankadari, J.A. Wilce, Emerging COVID-19 coronavirus: glycan shield and structure prediction of spike glycoprotein and its interaction with human CD26, Emerging microbes & infections, 9 (2020) 601-604.
[2] K. Tian, M. Shao, Y. Wang, J. Guan, S. Zhou, Boosting compound-protein interaction prediction by deep learning, Methods, 110 (2016) 64-72.
[3] Y. Cai, M.J. Hossain, J.-K. Hériché, A.Z. Politi, N. Walther, B. Koch, M. Wachsmuth, B. Nijmeijer, M. Kueblbeck, M. Martinic-Kavur, Experimental and computational framework for a dynamic protein atlas of human cell division, Nature, 561 (2018) 411-415.
[4] J. Alex, J. Gary, Cosolute and Crowding Effects on a Side-By-Side Protein Dimer, Biochemistry, (2017).
[5] T. NAKANO, A. TERAWAKI, H. ARITA, INFLUENCE OF β-LACTAM ANTIBIOTICS ON PLATELETS. II. IN VITRO EFFECTS OF SOME β-LACTAM ANTIBIOTICS ON THE BIOCHEMICAL RESPONSES OF RAT PLATELETS, Journal of pharmacobio-dynamics, 10 (1987) 408-420.

[6] N. Malangu, Poisoning: From Specific Toxic Agents to Novel Rapid and Simplified Techniques for Analysis, BoD–Books on Demand, Place Published, 2017.
[7] P. Taboada, D. Attwood, J.M. Ruso, M. García, F. Sarmiento, V. Mosquera, Effect of electrolyte on the surface and thermodynamic properties of amphiphilic penicillins, Journal of colloid and interface science, 220 (1999) 288-292.
[8] P. Taboada, D. Attwood, J.M. Ruso, M. García, F. Sarmiento, V. Mosquera, Influence of molecular structure on the ideality of mixing in micelles formed in binary mixtures of surface-active drugs, Journal of colloid and interface science, 216 (1999) 270-275.
[9] J. Ruso, D. Attwood, M. Garcia, P. Taboada, L. Varela, V. Mosquera, A study of the interaction of the amphiphilic penicillins cloxacillin and dicloxacillin with human serum albumin in aqueous solution, Langmuir : the ACS journal of surfaces and colloids, 17 (2001) 5189-5195.
[10] P. Taboada, D. Attwood, J.M. Ruso, F. Sarmiento, V. Mosquera, Self-association of amphiphilic penicillins in aqueous electrolyte solution: a light-scattering and NMR study, Langmuir : the ACS journal of surfaces and colloids, 15 (1999) 2022-2028.
[11] N. FUNAsAKI, S. HADA, S. NEYA, Self-association of penicillins in aqueous solution as revealed by gel filtration chromatography, Chemical and pharmaceutical bulletin, 42 (1994) 779-785.
[12] P. Taboada, V. Mosquera, J.M. Ruso, F. Sarmiento, M.N. Jones, Interaction between penicillins and human serum albumin: a thermodynamic study of micellar-like clusters on a protein, Langmuir : the ACS journal of surfaces and colloids, 16 (2000) 934-938.
[13] P. Taboada, V. Mosquera, J.M. Ruso, F. Sarmiento, M.N. Jones, Interaction between penicillins and human serum albumin: a ζ-potential study, Langmuir : the ACS journal of surfaces and colloids, 16 (2000) 6795-6800.
[14] N. Hassan, J.M. Ruso, P. Somasundaran, Mechanisms of fibrinogen–acebutolol interactions: Insights from DSC, CD and LS, Colloids and Surfaces B: Biointerfaces, 82 (2011) 581-587.
[15] I. Pechik, S. Yakovlev, M.W. Mosesson, G.L. Gilliland, L. Medved, Structural basis for sequential cleavage of fibrinopeptides upon fibrin assembly, Biochemistry, 45 (2006) 3588-3597.
[16] S. Kim, P.A. Thiessen, E.E. Bolton, J. Chen, G. Fu, A. Gindulyte, L. Han, J. He, S. He, B.A. Shoemaker, PubChem substance and compound databases, Nucleic Acids Res, 44 (2016) D1202-D1213.
[17] J. Madrazo, J.H. Brown, S. Litvinovich, R. Dominguez, S. Yakovlev, L. Medved, C. Cohen, Crystal structure of the central region of bovine fibrinogen (E5 fragment) at 1.4-Å resolution, Proceedings of the National Academy of Sciences, 98 (2001) 11967-11972.
[18] A. Bratek-Skicki, P. Żeliszewska, J.M. Ruso, Fibrinogen: a journey into biotechnology, Soft Matter, 12 (2016) 8639-8653.
[19] S. Hochreiter, G. Klambauer, M. Rarey, Machine Learning in Drug Discovery, ACS Publications, 2018.
[20] X.-Y. Meng, H.-X. Zhang, M. Mezei, M. Cui, Molecular docking: a powerful approach for structure-based drug discovery, Current computer-aided drug design, 7 (2011) 146-157.
[21] S. Renner, S. Derksen, S. Radestock, F. Mörchen, Maximum common binding modes (MCBM): consensus docking scoring using multiple ligand information and interaction fingerprints, Journal of chemical information and modeling, 48 (2008) 319-332.
[22] S. Mitternacht, I.N. Berezovsky, Coherent conformational degrees of freedom as a structural basis for allosteric communication, PLoS computational biology, 7 (2011).

[23] T. Oliwa, Y. Shen, cNMA: a framework of encounter complex-based normal mode analysis to model conformational changes in protein interactions, Bioinformatics, 31 (2015) i151-i160.
[24] U. Emekli, D. Schneidman-Duhovny, H.J. Wolfson, R. Nussinov, T. Haliloglu, HingeProt: automated prediction of hinges in protein structures, Proteins: Structure, Function, and Bioinformatics, 70 (2008) 1219-1227.
[25] J.G. Greener, M.J. Sternberg, AlloPred: prediction of allosteric pockets on proteins using normal mode perturbation analysis, BMC bioinformatics, 16 (2015) 335.
[26] T. Wiseman, S. Williston, J.F. Brandts, L.-N. Lin, Rapid measurement of binding constants and heats of binding using a new titration calorimeter, Analytical Biochemistry, 179 (1989) 131-137.
[27] S. Preus, K. Kilså, F.-A. Miannay, B. Albinsson, L.M. Wilhelmsson, FRETmatrix: a general methodology for the simulation and analysis of FRET in nucleic acids, Nucleic Acids Res, 41 (2013) e18-e18.
[28] S. Preus, DecayFit—Fluorescence Decay Analysis Software 1.3, FluorTools, http://www.fluortools.com, (2014).
[29] H. Berman, J. Westbrook, Z. Feng, G. Gilliland, T. Bhat, H. Weissig, I. Shindyalov, P. Bourne, The protein data Bank nucleic acids research. 2000, Europe PMC free article][Abstract][Google Scholar], 235-242.
[30] G. Martínez-Rosell, T. Giorgino, G. De Fabritiis, PlayMolecule ProteinPrepare: A web application for protein preparation for molecular dynamics simulations, Journal of Chemical Information and Modeling, 57 (2017) 1511-1516.
[31] M.D. Hanwell, D.E. Curtis, D.C. Lonie, T. Vandermeersch, E. Zurek, G.R. Hutchison, Avogadro: an advanced semantic chemical editor, visualization, and analysis platform, Journal of cheminformatics, 4 (2012) 17.
[32] O. Trott, A.J. Olson, AutoDock Vina: improving the speed and accuracy of docking with a new scoring function, efficient optimization, and multithreading, Journal of computational chemistry, 31 (2010) 455-461.
[33] S. Forli, R. Huey, M.E. Pique, M.F. Sanner, D.S. Goodsell, A.J. Olson, Computational protein–ligand docking and virtual drug screening with the AutoDock suite, Nature protocols, 11 (2016) 905-919.
[34] A. Tao, Y. Huang, Y. Shinohara, M.L. Caylor, S. Pashikanti, D. Xu, ezCADD: A rapid 2D/3D visualization-enabled web modeling environment for democratizing computer-aided drug design, Journal of chemical information and modeling, 59 (2018) 18-24.
[35] V. Le Guilloux, P. Schmidtke, P. Tuffery, Fpocket: an open source platform for ligand pocket detection, BMC bioinformatics, 10 (2009) 1-11.
[36] W.P. Feinstein, M. Brylinski, Calculating an optimal box size for ligand docking and virtual screening against experimental and predicted binding pockets, Journal of cheminformatics, 7 (2015) 1-10.
[37] R.A. Laskowski, M.B. Swindells, LigPlot+: multiple ligand–protein interaction diagrams for drug discovery, ACS Publications, 2011.
[38] F. Tama, F.X. Gadea, O. Marques, Y.H. Sanejouand, Building-block approach for determining low-frequency normal modes of macromolecules, Proteins: Structure, Function, and Bioinformatics, 41 (2000) 1-7.
[39] L.-W. Yang, C.-P. Chng, Coarse-grained models reveal functional dynamics-I. elastic network models–theories, comparisons and perspectives, Bioinformatics and Biology Insights, 2 (2008) BBI. S460.

[40] B.H. Lee, S. Seo, M.H. Kim, Y. Kim, S. Jo, M.-k. Choi, H. Lee, J.B. Choi, M.K. Kim, Normal mode-guided transition pathway generation in proteins, PloS one, 12 (2017) e0185658.
[41] J.G. Greener, M.J. Sternberg, AlloPred: prediction of allosteric pockets on proteins using normal mode perturbation analysis, BMC bioinformatics, 16 (2015) 1-7.
[42] R.J. Worthington, C. Melander, Overcoming resistance to β-lactam antibiotics, The Journal of organic chemistry, 78 (2013) 4207-4213.
[43] J.M. Kollman, L. Pandi, M.R. Sawaya, M. Riley, R.F. Doolittle, Crystal structure of human fibrinogen, Biochemistry, 48 (2009) 3877-3886.
[44] J. Stourac, O. Vavra, P. Kokkonen, J. Filipovic, G. Pinto, J. Brezovsky, J. Damborsky, D. Bednar, Caver Web 1.0: identification of tunnels and channels in proteins and analysis of ligand transport, Nucleic Acids Res, 47 (2019) W414-W422.
[45] Z. Chen, X. Zhang, C. Peng, J. Wang, Z. Xu, K. Chen, J. Shi, W. Zhu, D3Pockets: a method and web server for systematic analysis of protein pocket dynamics, Journal of chemical information and modeling, 59 (2019) 3353-3358.
[46] I. Sánchez-Linares, H. Pérez-Sánchez, J.M. Cecilia, J.M. García, High-throughput parallel blind virtual screening using BINDSURF, BMC bioinformatics, 13 (2012) S13.
[47] N.E. Newell, Mapping side chain interactions at protein helix termini, BMC bioinformatics, 16 (2015) 231.
[48] A. Bachmann, D. Wildemann, F. Praetorius, G. Fischer, T. Kiefhaber, Mapping backbone and side-chain interactions in the transition state of a coupled protein folding and binding reaction, Proceedings of the National Academy of Sciences, 108 (2011) 3952-3957.
[49] Z.-R. Xie, M.-J. Hwang, An interaction-motif-based scoring function for protein-ligand docking, BMC bioinformatics, 11 (2010) 298.
[50] R. Quiroga, M.A. Villarreal, Vinardo: A Scoring Function Based on Autodock Vina Improves Scoring, Docking, and Virtual Screening, PLOS ONE, 11 (2016) e0155183.
[51] V. Venkatraman, D.W. Ritchie, Flexible protein docking refinement using pose-dependent normal mode analysis, Proteins: Structure, Function, and Bioinformatics, 80 (2012) 2262-2274.
[52] O. Keskin, S.R. Durell, I. Bahar, R.L. Jernigan, D.G. Covell, Relating molecular flexibility to function: a case study of tubulin, Biophysical journal, 83 (2002) 663-680.
[53] C. Chennubhotla, A. Rader, L.-W. Yang, I. Bahar, Elastic network models for understanding biomolecular machinery: from enzymes to supramolecular assemblies, Physical Biology, 2 (2005) S173.
[54] F. Tama, Y.-H. Sanejouand, Conformational change of proteins arising from normal mode calculations, Protein engineering, 14 (2001) 1-6.
[55] R. Brüschweiler, Collective protein dynamics and nuclear spin relaxation, The Journal of chemical physics, 102 (1995) 3396-3403.
[56] K. Suhre, Y.-H. Sanejouand, ElNemo: a normal mode web server for protein movement analysis and the generation of templates for molecular replacement, Nucleic Acids Res, 32 (2004) W610-W614.
[57] P. Petrone, V.S. Pande, Can conformational change be described by only a few normal modes?, Biophysical journal, 90 (2006) 1583-1593.
[58] L. Yang, G. Song, R.L. Jernigan, Protein elastic network models and the ranges of cooperativity, Proceedings of the National Academy of Sciences, 106 (2009) 12347-12352.
[59] Y. Dehouck, A.S. Mikhailov, Effective harmonic potentials: insights into the internal cooperativity and sequence-specificity of protein dynamics, PLoS Comput Biol, 9 (2013) e1003209.

[60] P.M. Keen, The binding of penicillins to bovine serum albumin, Biochemical Pharmacology, 15 (1966) 447-463.
[61] K.E. Riley, J.S. Murray, J. Fanfrlík, J. Řezáč, R.J. Solá, M.C. Concha, F.M. Ramos, P. Politzer, Halogen bond tunability I: the effects of aromatic fluorine substitution on the strengths of halogen-bonding interactions involving chlorine, bromine, and iodine, Journal of Molecular Modeling, 17 (2011) 3309-3318.
[62] K.E. Riley, P. Hobza, Strength and Character of Halogen Bonds in Protein–Ligand Complexes, Crystal Growth & Design, 11 (2011) 4272-4278.
[63] A. Memic, M.R. Spaller, How Do Halogen Substituents Contribute to Protein-Binding Interactions? A Thermodynamic Study of Peptide Ligands with Diverse Aryl Halides, ChemBioChem, 9 (2008) 2793-2795.
[64] N. Hassan, L.R. Barbosa, R. Itri, J.M. Ruso, Fibrinogen stability under surfactant interaction, Journal of colloid and interface science, 362 (2011) 118-126.
[65] A. Cooper, M.A. Nutley, A. Wadood, Differential scanning microcalorimetry, Protein-ligand interactions: Hydrodynamics and calorimetry, (2000) 287-318.
[66] M. González-Durruthy, G. Scanavachi, R. Rial, Z. Liu, M.N.D.S. Cordeiro, R. Itri, J.M. Ruso, Structural and energetic evolution of fibrinogen toward to the betablocker interactions, International Journal of Biological Macromolecules, 137 (2019) 405-419.
[67] J. Marx, G. Hudry-Clergeon, F. Capet-Antonini, L. Bernard, Laser Raman spectroscopy study of bovine fibrinogen and fibrin, Biochimica et biophysica acta, 578 (1979) 107-115.
[68] M.M. Lopez, D. Kosk-Kosicka, Spectroscopic analysis of halothane binding to the plasma membrane Ca 2+-ATPase, Biophysical journal, 74 (1998) 974-980.
[69] A. Sułkowska, Interaction of drugs with bovine and human serum albumin, Journal of Molecular Structure, 614 (2002) 227-232.